AN INVESTIGATION OF ARRAY ELEMENTS FOR ENHANCED SINGLE ECHO ACQUISITION IMAGING

A Thesis

by

COLLEEN ELIZABETH DOMINICK

Submitted to the Office of Graduate Studies of
Texas A&M University
in partial fulfillment of the requirements for the degree of

MASTER OF SCIENCE

August 2005

Major Subject: Electrical Engineering

AN INVESTIGATION OF ARRAY ELEMENTS FOR ENHANCED SINGLE ECHO ACQUISITION IMAGING

A Thesis

by

COLLEEN ELIZABETH DOMINICK

Submitted to the Office of Graduate Studies of
Texas A&M University
in partial fulfillment of the requirements for the degree of

MASTER OF SCIENCE

Approved by:

Chair of Committee,	Steven Wright
Committee Members,	Jim Ji
	Krzysztof Michalski
	Hsin-i Wu
Head of Department,	Chanan Singh

August 2005

Major Subject: Electrical Engineering

ABSTRACT

An Investigation of Array Elements for Enhanced

Single Echo Acquisition Imaging. (August 2005)

Colleen Elizabeth Dominick, B.S., Texas A&M University

Chair of Advisory Committee: Dr. Steven M. Wright

Rapid MR imaging has facilitated the development of a variety of medical tools such as MR guided surgeries, drug delivery, stent placement, biopsies, and blood flow imaging. This rapid imaging is largely attributable to the development of parallel imaging techniques. In one such technique, single echo acquisition (SEA) imaging, scan time is reduced by substituting the lengthy phase encoding process with spatial information from an extensive receiver coil array. In order to easily construct and obtain images from this coil array, an ideal set of coil elements would be easily decoupled and tuned, possess high SNR and penetration depth, and would allow for operation in both transmit and receive mode. Several types of coils have been considered for use in massive coil arrays, including the planar pair coil, the loop coil and the stripline coil. This thesis investigates each of these coils for use in massive arrays for SEA imaging with enhanced penetration. This investigation includes: improving the currents on the planar pair coil, determining the feasibility of the loop coil and the stripline coil at the scale required for SEA, and comparing the salient properties of each coil type. This investigation revealed that the stripline coil appears to be the best coil element for SEA imaging with enhanced penetration.

To my mom,
with love and gratitude

ACKNOWLEDGEMENTS

I would like to express my gratitude towards Dr. Steven Wright, my research advisor, for his continuous guidance, support and enduring patience. I would also like to thank my committee members, Dr. Jim Ji, Dr. Krzysztof Michalski, and Dr. Hsin-i Wu. I would especially like to thank my colleagues in the MRSL, Dr. Mary McDougall, Hyokwon Nam, Naresh Yallapragada, Dan Spence and Susan Mathew. This thesis would not have been possible without your extensive knowledge, support, and humor.

Special thanks go to my family and friends for their love and support and to Juan for his never-ending encouragement and patience. Finally, I would like to thank my mom who always knew I could do it.

TABLE OF CONTENTS

CHAPTER Page

LIST OF FIGURES

FIGURE Page

FIGURE Page

FIGURE Page

LIST OF TABLES

CHAPTER I

INTRODUCTION

Rapid MR imaging has facilitated the development of a variety of medical tools such as MR guided surgeries, drug delivery, stent placement, biopsies, and blood flow imaging. This rapid imaging is largely attributable to the development of parallel imaging techniques that reduce MR scan times without increasing gradient demands by replacing time-consuming spatial encoding steps with spatial information inherent in a multiple-coil array. Our group has presented a completely parallel imaging technique, single echo acquisition (SEA), which uses a 64 element array of long, narrow coils and a 64-channel receiver to eliminate phase encoding altogether.

The 64 element array used in conjunction with SEA consists of planar pair coils, which exhibit inherently low coupling; this reduced coupling, however, comes at the expense of a non-uniform current distribution and a shallow penetration depth. Although this array is sufficient for surface imaging applications, deeper penetration is needed for deeper imaging applications. The primary aim of this research is to find a SEA element that would be better suited for deeper imaging applications. Options that were considered include improving the current distribution on the planar pair coil to gain penetration and investigating the feasibility of the loop coil and the microstrip transmission line (stripline) coil at the small scale required for SEA imaging.

The journal model is Concepts in Magnetic Resonance. Part B, Magnetic Resonance Engineering.

This research investigates each of these elements to determine which coil provides enhanced penetration depth without extreme complexity. This investigation proceeds in Chapter II with a presentation of the pertinent technical background. Chapter III discusses the modeling of the fields of the planar pair and the elimination of the full wave artifact. Chapter IV and Chapter V discuss the investigation of the loop coil and the stripline coil, respectively. In Chapter VI, the salient properties of the three coil types are compared and the stripline is selected as the SEA element. Finally, Chapter VII summarizes this research and discusses future work to be done.

CHAPTER II

THEORETICAL BACKGROUND

II.1 MR Image Formation

To form an MR image, the object to be imaged is placed in an external magnetic field so that a small majority of the hydrogen protons (spins) in the object align with the field (Figure 1). If the external field is along the z-axis, the protons aligned with the field are collectively referred to as the net magnetization, M_o. These protons precess about the axis of the external field at the resonance or Larmor frequency described by:

$$\omega = \gamma B_o \qquad (2.1)$$

where ω is the resonance frequency in MHz, γ is the gyromagnetic ratio, 42.56 MHz/Tesla for hydrogen, and B_o is the external magnetic field in Tesla. A radio frequency (RF) pulse is applied at the Larmor frequency, and the spins absorb this energy and move to a higher energy state or precess down to the x-y plane. Once the RF pulse is removed, the absorbed RF energy is emitted at the resonance frequency and the protons relax back to their original orientation along the z-axis. The RF energy that is emitted is recorded in time, and the Fourier transform of the signal is taken to determine its frequency content. The RF pulse is typically transmitted through a volume coil that surrounds the object being imaged; the return of the spins to their original position is received with the same volume coil or a separate surface coil. The surface coil can be localized to the object's region of interest and therefore produces images with a higher

signal-to-noise ratio (SNR). Without any gradients applied to the magnetic field, the emitted signal will be at a single frequency, corresponding to the chemical content of the object (i.e. water precesses at a different rate than fat).

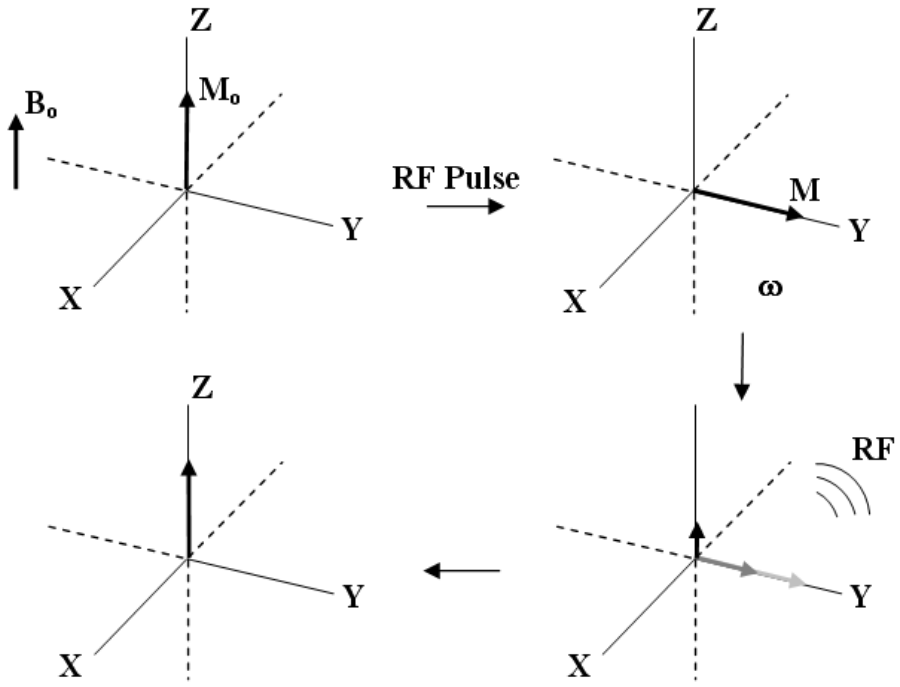

Figure 1: The path of the net magnetization in an MR experiment. The magnetization is initially aligned with the external magnetic field and is tipped to the y-axis flowing a 90° RF pulse. After the pulse, the magnetization relaxes back to its original orientation.

To spatially localize this signal to form an image, gradients are applied to the magnetic field to map the frequency of the spins to their position in the magnet. First, a gradient is applied to the external magnetic field along the z-direction, the slice select gradient, so that protons will precess faster or slower, based on their position along the slice. An RF pulse is simultaneously applied over the band of frequencies that

correspond to the slice that is to be imaged; only protons precessing at the frequencies included in the bandwidth of the RF pulse will be excited and therefore imaged. Dephasing of the spins occurs during the slice select gradient immediately after the spins are tipped to the x-y plane, however, so a slice "rephasing" gradient is applied immediately after the slice select gradient to put the spins back in phase. Next, a gradient is applied in the direction of the frequency encoding axis, so that the protons along this axis will be precessing at different frequencies based on their position, and the time domain signal is acquired; this is referred to as frequency encoding and does not increase the time needed to make a MR image. Frequency encoding only maps the frequencies of the protons to position along one axis; however, a second axis is required to form a two-dimensional image. This is accomplished by applying a gradient along a perpendicular axis that creates a position-dependent phase shift across the spins; this is referred to as phase encoding. The phase encoding gradient typically occurs before (or during) the frequency encoding gradient. To form the image resolution along the phase encoding axis, this whole sequence (slice select, excitation, frequency and phase encoding) must be repeated n times (typically 256 times) with n different phase encoding gradient amplitudes. After the time-domain signal is acquired during frequency encoding, a 2-dimensional Fourier transform is applied to form the image (*1*). A simplified pulse sequence depicting the above events can be seen in Figure 2.

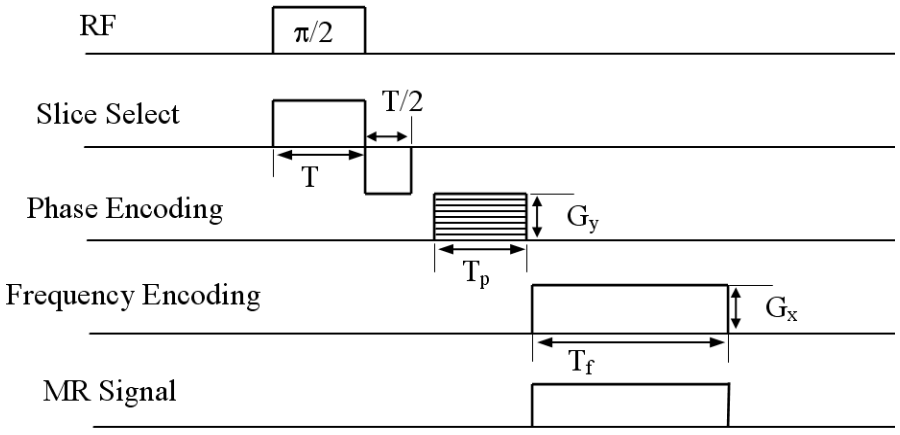

Figure 2: Simplified gradient echo pulse sequence.

The time-domain signal received during the nth repetition of the pulse sequence is described by the following equation:

$$S(k_x, k_y) = \iint_{slice} I(x,y) e^{+jk_y y} e^{+jk_x x} dxdy \qquad (2.2)$$

where:

$k_y = \gamma G_{y,n} T_p$

$k_x = \gamma G_x (t_f - t_{dephase})$

$G_{y,n}$ = the amplitude of the phase encode gradient used in the nth repetition

G_x = the amplitude of the frequency encode gradient

T_p = the length of the phase encode gradient

t_f = the time since the beginning of the frequency encode gradient

$t_{dephase}$ = the length of the frequency dephasing gradient, not shown in Figure 2

$I(x,y)$ = the signal from the object to be imaged.

In order to form an image with N_p by N_f resolution from this signal (where N_p is the resolution in the phase encode direction and N_f is the resolution in the frequency encode direction, typically 256 by 256), it is necessary to sample the signal N_f times during the frequency encode gradient and to repeat the sequence N_p times, with N_p different phase encode gradient values. This results in lengthy scan times to obtain an image with acceptable resolution; these times can be reduced by rapidly switching the gradients and by using higher power RF pulses and rapid pulse sequences. Although achievable with current technology, these approaches are limited in their effectiveness due to the physiological side effects that result (*2*). An alternative to using faster gradients is to use spatial information from multiple receiver coils to synthesize phase encoding steps (lines); this is referred to as parallel imaging. For example, a fewer number of phase encode lines are acquired to cover the same field of view (FOV) in a shorter time and the remaining phase encode lines are synthesized using spatial information inherent in the surface coil's sensitivity patterns. Unlike gradient dependent reduction techniques, this method relies on the sensitivity of the receivers and does not affect the object being imaged.

II.2 Parallel Imaging in MRI

The concept of using multiple coils to simultaneously acquire an image was suggested by Hyde et al as a means to improve the SNR of an image without reducing the FOV (*3*). Roemer et al successfully demonstrated this technique by simultaneously acquiring independent data from multiple receive coils and then combining the data to form images with high SNR over a large FOV (*4*). These early methods led to the notion

of using the independent data from multiple receive coils not only to improve SNR but also to synthesize phase encode lines to reduce imaging times (*5-8)***.** Although many techniques for image reconstruction were hypothesized, parallel imaging was first successfully reported by Sodickson et al with the SMASH method (Simultaneous Acquisition of Spatial Harmonics) (*9*). This technique uses weighted sensitivity patterns from multiple receive coils to synthesize phase variations in the signal normally impressed by phase encode gradients (*10*). SENSE (Sensitivity Encoding), another parallel technique introduced by Pruessmann et al, also uses sensitivity patterns from receive coils to synthesize phase encode lines, but it allows for a more flexible coil geometry than SMASH (*11*). A number of other parallel imaging techniques, including PILS (Parallel Imaging with Localized Sensitivity Profiles) (*12*), Space Rip (Sensitivity Profiles from an Array of Coils for Encoding and Reconstruction in Parallel) (*13*), and GRAPPA (Generalized Autocalibrating Partially Parallel Acquisitions) (*14*) have been proposed. Like SMASH and SENSE, these are all partially parallel imaging techniques that use an array of N coils to theoretically reduce the imaging time by a factor of N; in practice, the acceleration factor is typically less than the coil number however (*10*). Another parallel imaging modality introduced by Wright et al, SEA uses an extensive receive array to acquire an image in a single echo with no phase encoding gradients (*15*). This technique requires a unique receive coil array and is discussed in detail in II.4.

For any of the above mentioned parallel imaging techniques to produce an acceptable image, the multiple surface coils in the receive array each must receive a unique signal; this requires that the mutual impedance between all of the coils be

negligible so that current in one coil does not induce a voltage in another coil (coil coupling) (*3*). The mutual impedance between two coils is:

$$Z_{jk} = \left.\frac{V_j}{I_k}\right|_{Ij=0}. \qquad (2.3)$$

A simple way to minimize the mutual impedance between coils is to space them sufficiently far apart, but this is not feasible for parallel imaging techniques. Other more practical options are to overlap adjacent coils, to use transformers between adjacent coils or to place capacitors between coils. Coupling can be further reduced between adjacent and non-adjacent coils by connecting the coils to low input impedance preamplifiers. The low input impedance preamplifier in series with a proper value inductor creates a parallel resonant circuit with the match capacitor of the coil (Figure 3). If the input impedance of the preamp is low enough (< 3Ω), the resonant circuit will prevent current flow in the coil, thus inhibiting coupling to neighboring coils, yet still transmitting the MR signal to the preamplifier (*4*).

Another option used to reduce coupling between coils is to add a balun (balanced to unbalanced) to the feed of the coil. The balun makes the unbalanced coaxial cable a balanced feed by eliminating stray currents on the shield of the coaxial cable; having a balanced feed ensures that the currents on the coil will be symmetric thus removing coupling due to improper currents. There are several types of baluns that are commonly used, including the cable-trap balun, the quarter-wavelength balun and the lattice balun.

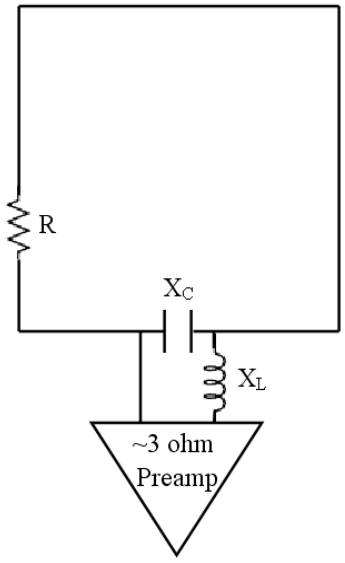

Figure 3: A low input-impedance preamplifier decoupling scheme.

$$X_L = X_C = \sqrt{50R} \quad (4)$$

II.3 MR Surface Coils

As mentioned previously, a key component of any parallel imaging technique is the receive coil array. These arrays are typically composed of numerous, independent surface coil elements oriented in a manner conducive to producing images with a high SNR. There are numerous types of surface coils, including the loop coil, the planar pair coil and the stripline coil.

II.3.1 Loop Coil

The loop coil is the standard MR receive coil; the loop coil that would be used for SEA imaging has a rectangular conductor with a gap for the feed (Figure 4). The fields of a loop can be approximated using a quasi-static approach; in MR literature and

in this thesis, the "fields" of a coil is used to refer to the flux density, B. By assuming a constant current distribution I, the fields of the loop can be easily found using the Biot-Savart Law:

$$\vec{B} = \frac{\mu I}{4\pi}\int \frac{d\vec{l} \times \hat{a}_R}{R^2} \tag{2.4}$$

where μ is the permeability of free space, R is the distance from the position along the loop to the position where the fields are being calculated, and $\hat{a}_R$ is the unit vector directed from the position along the loop to the position where the fields are being calculated. For a z-directed finite segment of current, such as a segment of a loop, the closed form of equation 2.4 is:

$$\vec{B} = \frac{\mu I}{4\pi\rho}\left[\frac{z - z_A}{R_A} - \frac{z - z_B}{R_B}\right]\hat{a}_\phi \tag{2.5}$$

where z_A is the lower limit of the segment, z_B is the upper limit of the segment, $\rho = \sqrt{x^2 + y^2}$, $R_A = \sqrt{\rho^2 + (z - z_A)^2}$, and $R_B = \sqrt{\rho^2 + (z - z_B)^2}$. Equation 2.5 is easily extended to compute the fields for x or y directed segments of current, and the total field is found by summing the contribution from each segment of the loop. The normalized field magnitude of the loop taken across the coil and as the distance above the coil increases can be seen in Figure 5. The fields were computed using a full wave program previously developed in-house (*16*).

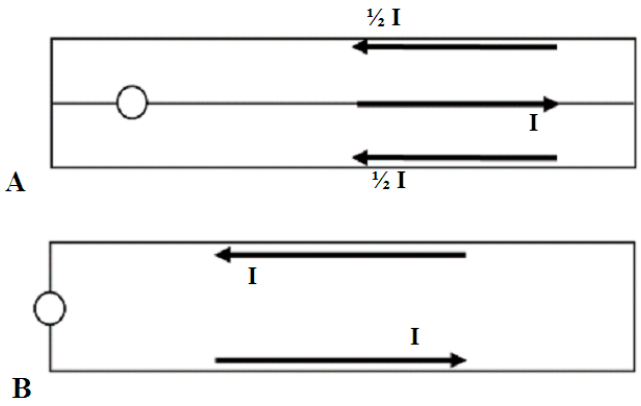

Figure 4: Schematic of a planar pair coil (A) and a loop coil (B).

II.3.2 Planar Pair Coil

The planar pair coil is composed of two side-by-side loop coils with a shared center conductor and is fed on the center conductor such that current travels up the center conductor, splits and returns on the outer legs (Figure 4). The fields of the planar pair coil can again be analyzed using the Biot-Savart Law, assuming a current of I on the center leg and ½ I on the outer legs. The normalized field magnitude of the planar pair taken across the coil and as the distance above the coil increases can be seen in Figure 5. It is evident from the field patterns of both coils that the field of the planar pair coil is much shallower and narrower than the field of the loop coil.

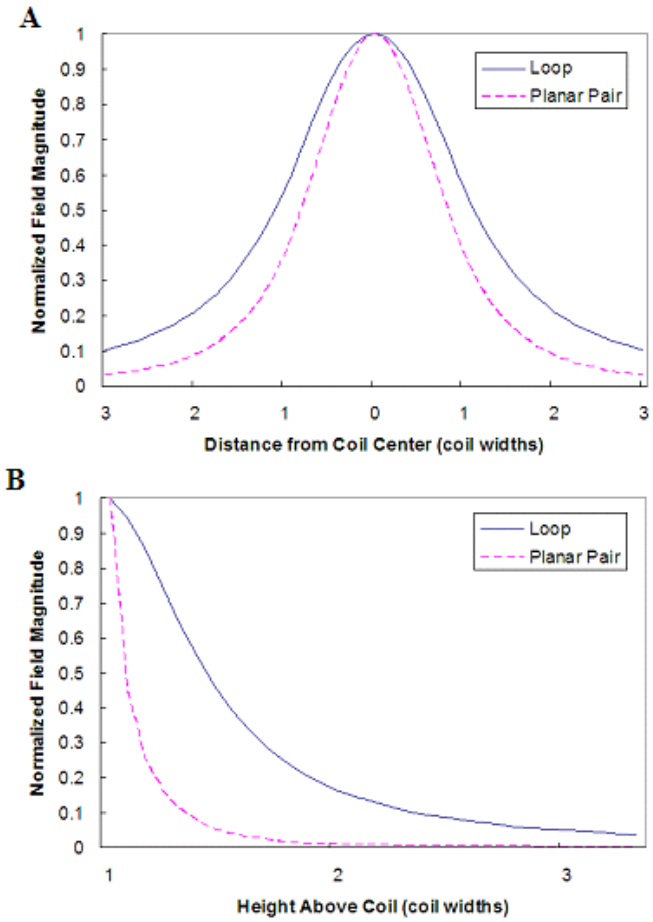

Figure 5: Modeled field magnitudes of the planar pair and loop coil. (A) Normalized field magnitude taken across the coil at one coil width above the coil. (B) Normalized field magnitude taken in the center of the coil as the distance above the coil increases.

II.3.3 Stripline Coil

Although the planar pair coil and the loop coil are widely reported, the stripline coil is a newly reported MR phased array detector (*17-19*). Previously, linear elements similar to striplines were only employed in single-channel detectors, such as birdcage coils (*20*), but had not been employed as independent detector elements in multi-channel receive arrays (*17*). The stripline element was first reported for use multi-channel arrays

by Lee et al as a λ/4 length or λ/2 length linear strip element embedded in a high permittivity dielectric over a ground plane (*17*). The stripline element has also been reported for receive arrays by Zhang et al as a λ/2 length thin strip conductor over a ground plane separated by a low-loss dielectric, but to make the element a reasonable size for an MR detector, the strip is arranged in a loop style configuration (*18*). A similar style stripline coil has been reported by Adriany et al for transmit and receive imaging at 7 Tesla in both a linear and a loop style configuration (*19*). Adriany et al use an additional tune capacitor to allow for more flexibility in the length of the coil, however.

The stripline is widely reported in RF/Microwave circuit design and is formed by sandwiching a dielectric substrate between a strip conductor and a ground plane (*21*). Because the stripline is half-shielded (i.e. exposed to both air and dielectric), the stripline is considered to operate in a quasi-transverse electromagnetic mode for frequencies of interest in MRI. Although numerous analyses of the stripline have been performed, the quasistatic solution developed by Bahl et al uses approximations that are applicable to the MR stripline to develop empirical design equation formulas for the stripline (*21-24*). This derivation is found in (*18*) and is repeated below.

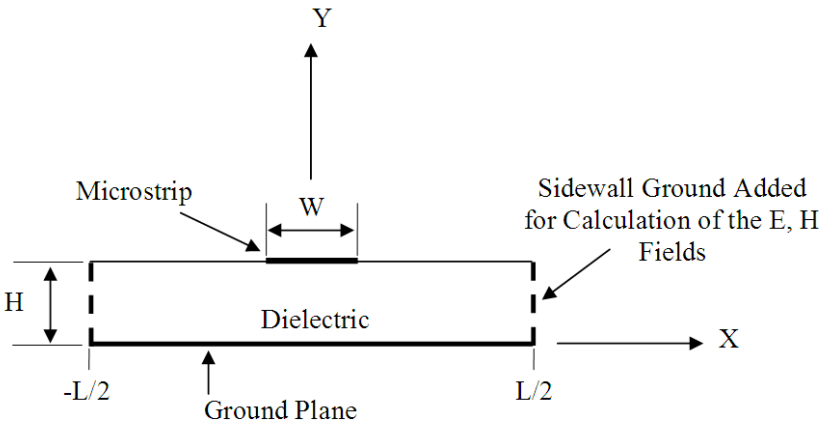

Figure 6: End view of a microstrip transmission line coil. H is the dielectric heigth, W is the width of the microstrip, and L is the length of the ground plane.

To simplify the analysis of the stripline, the ground plane is extended up the sides of the dielectric. Because the length of the dielectric and ground plane, L, is much larger than the dielectric height, H, and the field lines are localized to the stripline, the addition of the grounded sidewalls does not perturb the stripline (Figure 6). As described in (*18*), the scalar potential, $\Phi(x,y)$, must be zero at the ground sidewalls. Therefore, the boundary conditions to Laplace's equation are:

$$\vec{E} = -\nabla\Phi = 0 \text{ and } \Phi(x,y) = 0 \text{ at } x = \pm\frac{L}{2} \text{ and/or } y = 0,\infty . \qquad (2.6)$$

Which satisfies Laplace's equation:

$$\nabla^2\Phi(x,y) = 0 \text{ for } |x| \le \frac{L}{2} \text{ and } 0 \le y < \infty . \qquad (2.7)$$

The solution to Laplace's equation is then found through separation of variables and is:

$$\Phi(x,y) = \sum_{k=1,odd}^{\infty} A_k \cos\frac{k\pi x}{L}\sinh\frac{k\pi y}{L}, \text{ for } 0 \le y < H \qquad (2.8)$$

and:

$$\Phi(x,y) = \sum_{k=1,odd}^{\infty} B_k \cos\frac{k\pi x}{L}\exp\frac{-k\pi y}{L}, \text{ for } H \le y < \infty \qquad (2.9)$$

where A_k and B_k are related coefficients. B_k is found by equating equations 2.8 and 2.9 at y = H and is:

$$B_k = A_k \sinh\frac{k\pi H}{L}\exp\frac{k\pi H}{L}, \text{ for } y = H. \qquad (2.10)$$

Therefore equation 2.9 can be rewritten as:

$$\Phi(x,y) = \sum_{k=1,odd}^{\infty} A_k \cos\frac{k\pi x}{L}\sinh\frac{k\pi H}{L}\exp\frac{k\pi H - k\pi y}{L}, \text{ for } H \le y < \infty. \qquad (2.11)$$

A_k is found by evaluating the surface charge density, ρ, on the stripline at $y = H^+, H^-$:

$$\rho = \varepsilon_o E_{y|_{y=H^+}} - \varepsilon_o \varepsilon_r E_{y|_{y=H^-}} \qquad (2.12)$$

where

$$E_y = -\frac{\partial\Phi(x,y)}{\partial y} \qquad (2.13)$$

and ε_o, ε_r are the permittivity of free space and the dielectric, respectively. For the stripline, the charge density can be approximated as 1 on the strip and 0 outside of it; this is a valid assumption for MR experiments which occur at relatively low frequencies and can assume constant current distributions. A_k is then found to be:

$$A_k = \frac{4L \sin \frac{k\pi W}{2L}}{\varepsilon_o k^2 \pi^2 \left(\varepsilon_r \cosh \frac{k\pi H}{L} + \sinh \frac{k\pi H}{L} \right)}. \qquad (2.14)$$

Therefore, equations 2.8, 2.9, 2.10 and 2.14 give the general solution to the scalar potential (*18*). The electric and magnetic fields are then found using a quasi-statics approach from:

$$\vec{E} = -\nabla\Phi \bullet e^{j\omega t} \text{ and } \vec{H} = \frac{-1}{j\omega\nabla \times \vec{E} \bullet e^{j\omega t}}. \qquad (2.15 \text{ a, b})$$

These fields can be used to derive the design equations for the stripline, assuming that the stripline thickness is negligible compared to the dielectric thickness (*24*). The resonance wavelength of the microstrip is:

$$\lambda = \frac{\lambda_o}{\sqrt{\varepsilon_{eff}}} \qquad (2.16)$$

where λ_o is the wavelength of light in free space and the effective dielectric constant is:

$$\varepsilon_{eff} = \frac{\varepsilon_r + 1}{2} + \frac{\varepsilon_r - 1}{2\sqrt{1 + \frac{12H}{W}}} + 0.02(\varepsilon_r - 1)\left(1 - \frac{W}{H}\right)^2, \text{ for W/H} \leq 1$$

and (2.17 a,b)

$$\varepsilon_{eff} = \frac{\varepsilon_r + 1}{2} + \frac{\varepsilon_r - 1}{2\sqrt{1 + \frac{12H}{W}}}, \text{ for W/H} > 1.$$

The characteristic impedance of the stripline is:

$$Z_o = \frac{60}{\sqrt{\varepsilon_{eff}}} \ln\left(\frac{8H}{W} + \frac{W}{4H}\right), \text{ for W/H} \le 1$$

and

$$Z_o = \frac{120\pi}{\sqrt{\varepsilon_{eff}}\left(\frac{W}{H} + 1.393 + 0.667\ln\left(\frac{W}{H} + 1.444\right)\right)}, \text{ for W/H} > 1 \qquad (2.18\text{ a,b})$$

where W is the stripline width and H is the dielectric height, demonstrated in Figure 6.

Coupling between two microstrip coils spaced a distance S apart can be described by the coupling coefficient, K_c:

$$K_C = \frac{j(Z_{0e} - Z_{0o})\sin\beta L}{2\cos\beta L + j(Z_{0e} + Z_{0o})\sin\beta L} \qquad (2.19)$$

where β is the propagation constant, $2\pi/\lambda_o$, and Z_{0e} and Z_{0o} are the even and odd modes of the characteristic impedance of the two microstrip lines. Z_{0e} and Z_{0o} are:

$$Z_{0e} = \frac{60}{Z_0\sqrt{\varepsilon_{eff}}}\left(\ln 2 + \ln\frac{1 + \tanh\left(\frac{\pi W}{2H}\right)\tanh\left(\frac{\pi}{2}\cdot\frac{W+S}{H}\right)}{1 - \tanh\left(\frac{\pi W}{2H}\right)\tanh\left(\frac{\pi}{2}\cdot\frac{W+S}{H}\right)}\right)$$

and (2.20 a,b)

$$Z_{0o} = \frac{60}{Z_0\sqrt{\varepsilon_{eff}}}\left(\ln 2 + \ln\frac{1 + \tanh\left(\frac{\pi W}{2H}\right)\coth\left(\frac{\pi}{2}\cdot\frac{W+S}{H}\right)}{1 - \tanh\left(\frac{\pi W}{2H}\right)\coth\left(\frac{\pi}{2}\cdot\frac{W+S}{H}\right)}\right).$$

Therefore, two side-by-side microstrips are decoupled when the strip width and the spacing between strips is greater than twice the dielectric height, i.e. $W+S \geq 2H$, because Z_{0e} is approximately equal to Z_{0o} and K_c is then zero (*17*,*25*). If this criterion, $W+S \geq 2H$, is not met there will be coupling between the striplines; it has been shown, however, that this coupling can be reduced to acceptable levels by placing lumped element capacitors between neighboring strips (*19*).

Stripline arrays with multiple, independent elements have been reported by Lee et al (*17*) and Adriany et al (*19*). The 8-channel stripline coil array reported by Adriany consists of striplines whose conducting strip and ground strip are oriented into rectangular loop shapes; the striplines are tuned to their resonance frequency by placing a tune capacitor between the conducting strip and the ground strip, and the match capacitor is placed between the conducting strip and the coaxial transmission line. This array, whose elements are approximately 20 times wider than would be desired for SEA imaging, exhibits at least 19 dB of decoupling between nearest neighbors. This decoupling is a combination of inherent broadband decoupling and capacitive decoupling between elements. The ease of decoupling the stripline coils makes it a viable option for SEA coil arrays.

II.4 SEA Imaging

As mentioned previously, SEA imaging uses receive coil sensitivity patterns from an extensive receive array to eliminate phase encoding altogether. Currently, SEA can produce images with a resolution of 64 by 256 in a single echo (*15*). Initial work has been reported by McDougall investigating the capabilities and limitations of the SEA

method and its corresponding RF coil array; a brief summary of the SEA method, initial work, and future goals are discussed in the following sections (*26*).

II.4.1 SEA Imaging Method

As described in II.1, in order to form a traditional N_p by N_f MR image, an RF pulse and gradients are applied, the resulting echo is acquired and sampled N_f times, and the whole procedure is repeated N_p times with N_p different phase encode gradient values. In SEA imaging, an RF pulse and gradients are applied and the resulting echo is acquired and sampled N_f times, but the procedure is only done once. The resolution in the phase encoding direction is formed in a single echo using the spatial information acquired simultaneously from long, narrow coils in a receive array. Currently, a 64-channel array of independent coils and a corresponding 64-channel receiver system are used to form the resolution in the phase encode direction, allowing for 64 by 256 images to be formed in a single echo.

To produce SEA images, the coil array is placed inside the magnet with each coil element aligned parallel to the z-axis of the magnet; frequency encoding is done along this axis. An RF pulse is applied for excitation and a single gradient pulse is applied in the phase encode direction to compensate for the phase across each receive coil (*27*). Echoes from each of the 64 coils are then simultaneously acquired by a corresponding channel in the 64-channel receiver, mixed to an intermediate frequency of 500 KHz and digitized with 16-bit resolution at 2.5MHz. The echoes are then digitally demodulated and a 1D-FFT is performed on each echo (*25,28-29*). Phase encoding is not performed; instead the transformed echoes from each coil in the array are stacked into adjacent rows

of a matrix, as each individual phase encode repetition would be, and interpolated to form a 256 by 256 image. Slices are selected parallel to the array, along the y-axis (Figure 7). A separate transmit coil is used for excitation, and the 64-channel array is used for receiving.

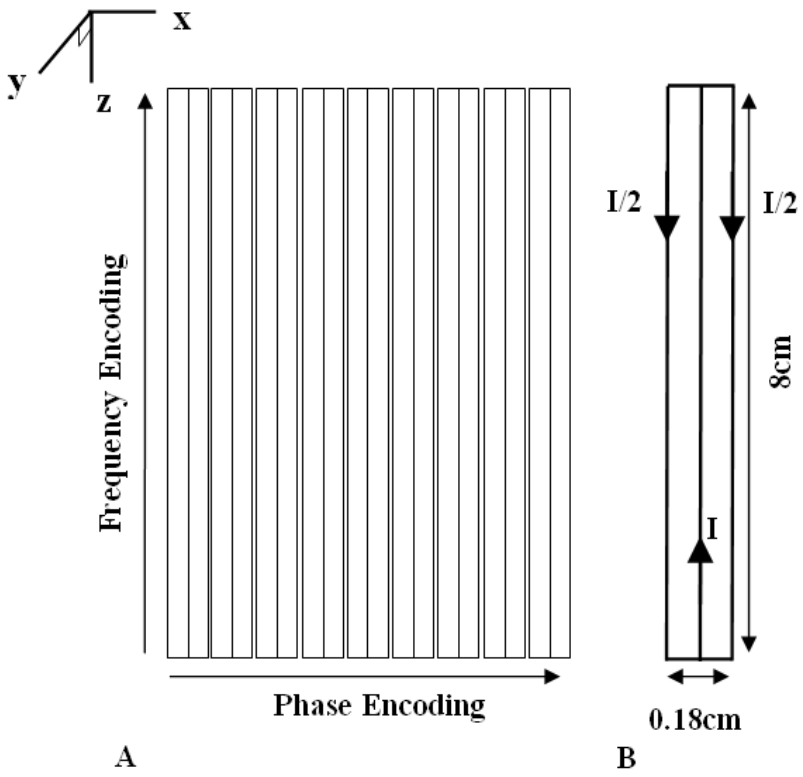

Figure 7: (A) A simplified schematic of the SEA coil array showing its orienation with respect to the axes of the magnet and the directions for phase and frequency encoding. (B) A schematic of the planar pair coil showing the flow of current and the dimensions.

The resolution in the array encoded image is limited by the individual element pattern, so the SEA method works best with narrow coils that have a narrow field pattern (*15*). The coils currently used for SEA are approximately 8cm long and 1.8mm wide, a

much different scale than traditional MR coils. Also, like many other parallel imaging techniques, it is important to have coils that are decoupled from one another to maximize coil sensitivity and SNR. Because of the number of coils that are used in SEA and the limited space, however, decoupling coils becomes an even more cumbersome task than with typical parallel imaging techniques. The planar pair coil was selected as the prototype coil element for SEA imaging due to its extremely narrow field pattern and inherent decoupling between elements (*26*).

II.4.2 SEA Coil Array

As demonstrated in II.3.2, the current distribution on the planar pair results in a very narrow field pattern and hence low coupling between elements. The array presently used for SEA imaging consists of 64 planar pair coils and is approximately 8.1cm long by 13cm wide. The single elements in the array are 8.1cm long by 1.8mm wide with 0.25mm spacing between elements. Each individual element consists of 0.25mm wide legs with 0.5mm gaps between the legs. The final version of the array has the tuning and matching networks at the coil and tuning is done using varactors. Ultrasound cable is used to transfer the signal from the coils to the preamplifiers (*26*,*30*-*31*). Although this array possesses the narrow field patterns and the low coupling between elements required for SEA imaging and has been used to successfully demonstrate the capabilities of the SEA technique, several limitations of this current array have become apparent. One issue with the array is that an artifact can be seen in some of the images taken with it**;** the artifact appears as a dark strip near the feed end of the coil and increases in size as the distance above the coil increases. This artifact is believed to be caused by a full wave

effect, resulting in a non-uniform current distribution on the coil (*26*). A second issue with the planar pair array is that it has a very shallow penetration depth. This shallow penetration was somewhat expected, due to the contained field pattern of the planar pair element but is made worse by the above mentioned artifact. Since this shallow penetration limits the SEA imaging applications, it is desired to eliminate the artifact seen with the current coil and also to explore other coil types for use in SEA imaging to achieve deeper penetration.

II.4.3 SEA Imaging Goals

One immediate goal for SEA imaging is to produce arrays that can be placed in other arrangements, such as two stacked planar arrays or a cylindrical array. These arrangements would obviously be benefited by using a coil element with greater penetration. Also, as mentioned above, a gradient pulse applied across the coil is required in SEA imaging to cancel the phase across the receive coil. Because the phase across the coil changes as the distance above the coil increases, the compensation gradient also changes with distance above the coil. Compensating for the phase across each coil becomes much more difficult, if not impossible, when the coils in the array are not linear, as is the case in a cylindrical array. When the coils in the array are used for both transmit and receive, however, the compensation gradient is no longer necessary. In addition, decoupling the receive array from the volume coil becomes much more complicated when the receive array is no longer linear. These considerations necessitate the development of a SEA array that can be used for both transmit and receive (*32*). The current array element, the planar pair, could be used in transmit and receive mode if the

tuning mechanism for the coils was changed to a fixed capacitance value, but deeper penetration than the planar pair currently has is preferred.

CHAPTER III

PLANAR PAIR COIL

The first step to improving the penetration depth of the SEA coil array was to verify the source of artifact seen with the present coil and to eliminate the artifact. The following chapter describes the modeling that was done to verify the source of the artifact and to test configurations to eliminate the artifact, the construction and testing of the proposed solution and the implementation of the solution in the array environment.

III.1 Procedures

III.1.1 Modeling the Currents on the Planar Pair Coil

To verify that the artifact seen in planar pair images is a full wave effect due to current non-uniformity, the complex currents on a planar pair element from the 4.7T SEA array were modeled at 200MHz using an in-house, full wave modeling program. A dielectric constant of 4.6 was used to simulate the coil substrate, G10; a thin layer of plastic (ε_r=2.2) and water were placed above the coil to simulate the phantom. These currents were then used to model the magnetic field produced by the coil, and the intensity and the phase of the field were plotted at various heights above the coil. The modeled currents showed an increase in current magnitude indicative of a full wave effect. Since one solution to full wave effects is to place capacitors breaking up the length of the coil, the currents on the coil and the magnetic field produced by the currents were modeled again, using the same program, but with capacitors added to the coil. The first configuration modeled was a capacitor at the far end of the center leg,

right before its split; this is position A in Figure 8. The currents and the resulting field were modeled with numerous capacitance values at this location. Various capacitor values were also placed at the far end of the outer legs of the coil (position B in Figure 8), the feed end of the outer legs (position C in Figure 8), and at the feed and far end of the outer legs (position B and C in Figure 8), and the currents and their resulting magnetic field were modeled for each capacitor value at each location.

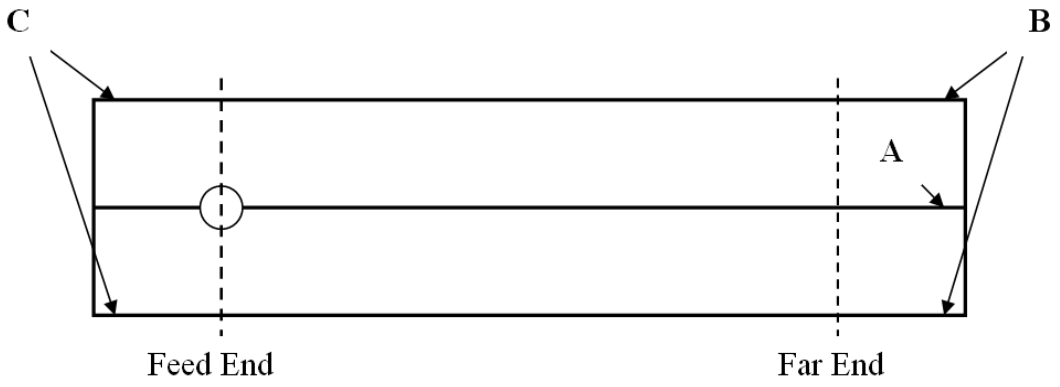

Figure 8: Capacitor placement for modeling the currents of the planar pair coil.

III.1.2 Constructing and Testing the Proposed Solution

Once a projected solution for the artifact was developed using the data from the modeling program, a planar pair coil with the proposed solution was constructed and tested. A coil identical to those in the center of the 64-channel array, but with a 15pF capacitor added to the feed end of the outside legs of the coil, was fabricated using the C30 PC board prototyper (LPKF, Wilsonville, OR) and tuned using the HP 4195A network analyzer. The added capacitance in the legs increased the capacitance needed to

tune the coil to 50Ω. A single planar pair coil identical to those in the center of the 64-channel array was also fabricated and tuned for comparison; both coils can be seen in Figure 9.

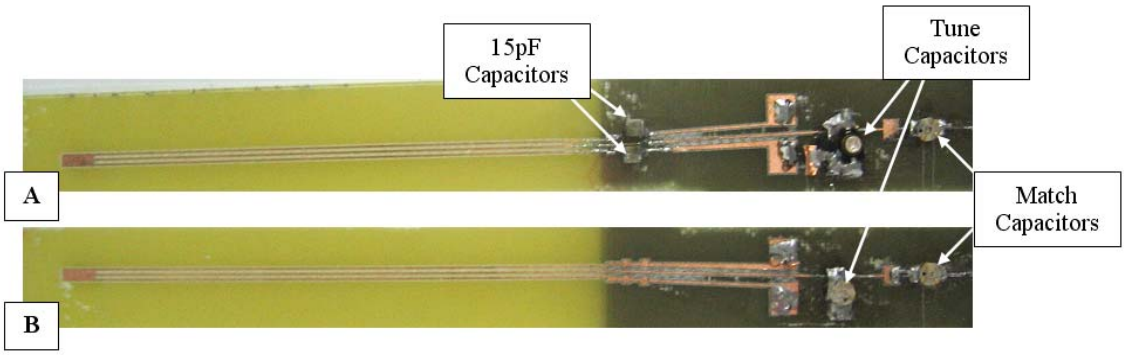

Figure 9: (A) Planar pair coil with capacitors added to remove the field artifact. (B) A unmodified planar pair coil used for comparison.

Axial images were then taken on the 4.7 T Omega system with the normal planar pair and the modified planar pair to verify that the artifact seen with the normal coil was no longer present with the modified planar pair and also to obtain the field patterns of both coils. MATLAB code was also written to compare the penetration depth and SNR of the two coils. Once the modification was demonstrated to have removed the artifact on a single coil, the modification was implemented on the 64-channel scale. The 64-channel coil design currently used for SEA imaging was modified by another member of the Magnetic Resonance Systems Lab (MRSL) to include capacitors on each outside leg at the feed end of the coil; vias from each leg were routed to the backside of the board and capacitors were placed on the backside to prevent interferences with the imaging

space on the top of the coil. This coil design was fabricated by PCB Express and matched and tuned in-house by another member of the MRSL.

III.2 Results

III.2.1 Modeling the Currents on the Planar Pair Coil

The computed currents on a planar pair element from the 4.7T SEA array can be seen in Table 1. An unexpected increase in the magnitude and the phase of the currents was seen from the feed end to the far end of the coil. These currents were then used to model the magnetic field produced by the coil, and the intensity and the phase of the field were plotted at various heights above the coil. The intensity images showed that the artifact did appear as the height above the coil increased, concurring with the image data from the 64-channel array. The phase ramp across the coil at the far end of the coil behaved as expected, decreasing with distance from the coil and remaining approximately 90 degrees directly above the coil. The phase across the coil at the feed end began to show unexpected behavior at a 5mm offset and no phase change at 7mm. Since the modeled currents produce the same artifact seen in the images with the SEA array, it was concluded that the artifact seen in the images is due solely to the currents on the coil. The modeled field intensity at various heights above the coil is seen in Figure 10, and the modeled field phase at various heights is seen in Figure 11.

Table 1 Modeled leg currents on the three legs of a planar pair at 200MHz.

Leg Currents	Outside Leg 1	Center Leg	Outside Leg 2
Magnitude (feed end)	2.528	4.973	2.528
Phase (feed end)	-88.716	91.321	-88.716
Magnitude (far end)	3.112	6.264	3.112
Phase (far end)	-89.49	90.528	-89.49

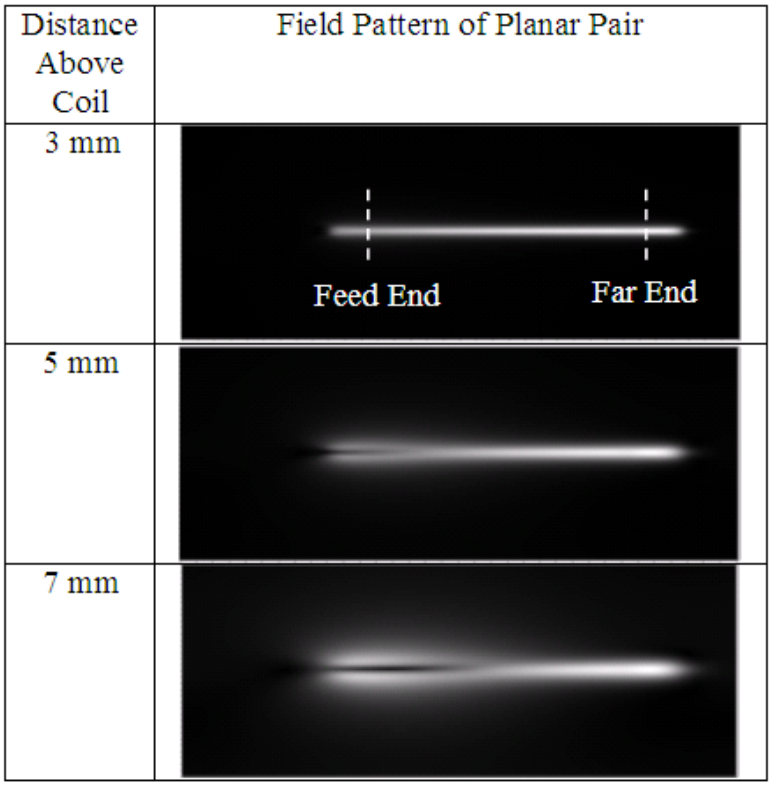

Figure 10: Modeled field intensity plots from a planar pair at various heights above the coil.

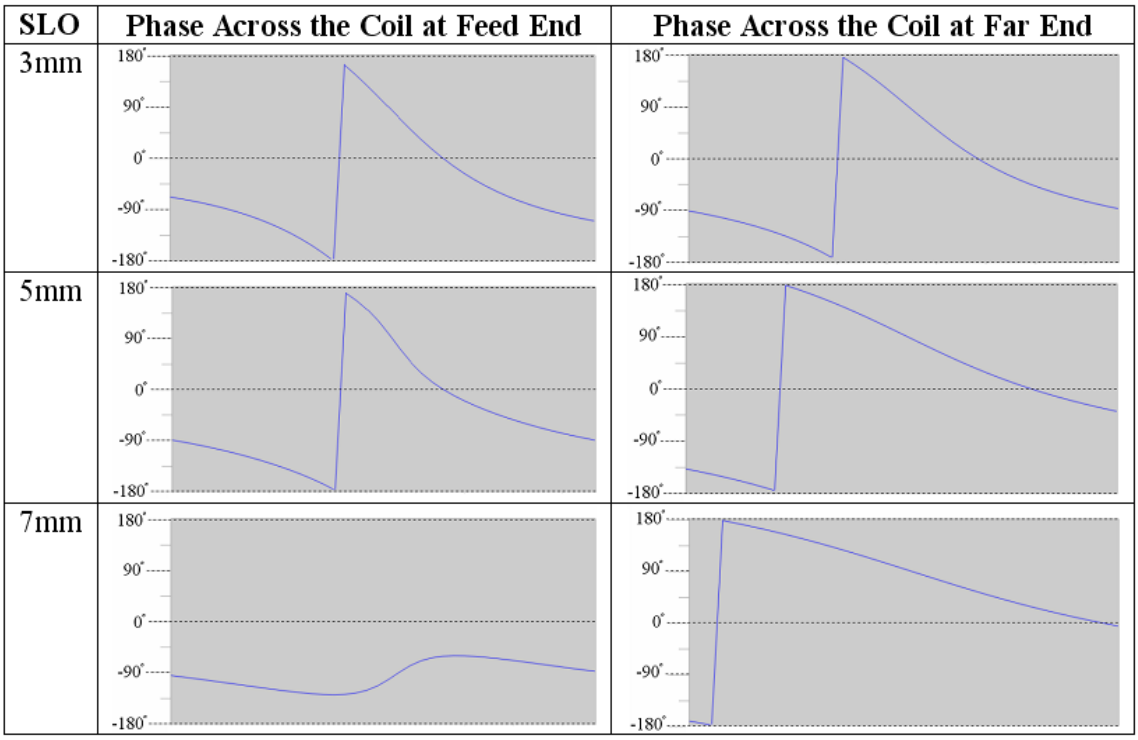

Figure 11: Modeled field phase plots from a planar pair coil at various heights above the coil.

To remove the artifact, capacitors were added at the various positions shown in Figure 8. The magnetic field was calculated from the computed currents for various capacitor values in position A, position B, position C and both position B and position C. For brevity, only the 7mm position, where the artifact is most apparent, is shown. The artifact appears to be most diminished with the capacitors in position C or in both position B and position C. Since the end goal is to implement the proposed solution on the 64-channel array, position C, which only uses two capacitors, seemed to be the best solution. The capacitor value that produces the optimal field pattern is 15pF; the currents resulting from this configuration are found in Table 2. The phase of the currents varies

dramatically less from end-to-end than the capacitor free case. Figure 12 shows the field magnitude for capacitors in position A and in position B; Figure 13 shows the field magnitude for various values in position C and for various values in both position B and position C. The field phase across the coil was also modeled from the currents and behaved as expected (Figure 14).

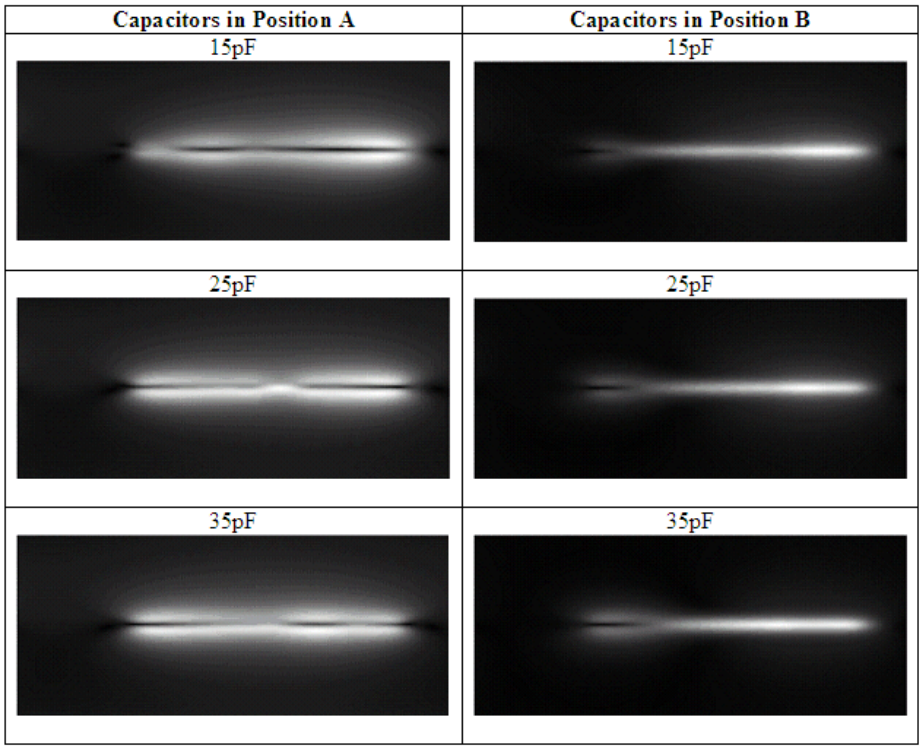

Figure 12: Modeled field magnitude 7mm above the coil with capacitors placed in position A and in position B.

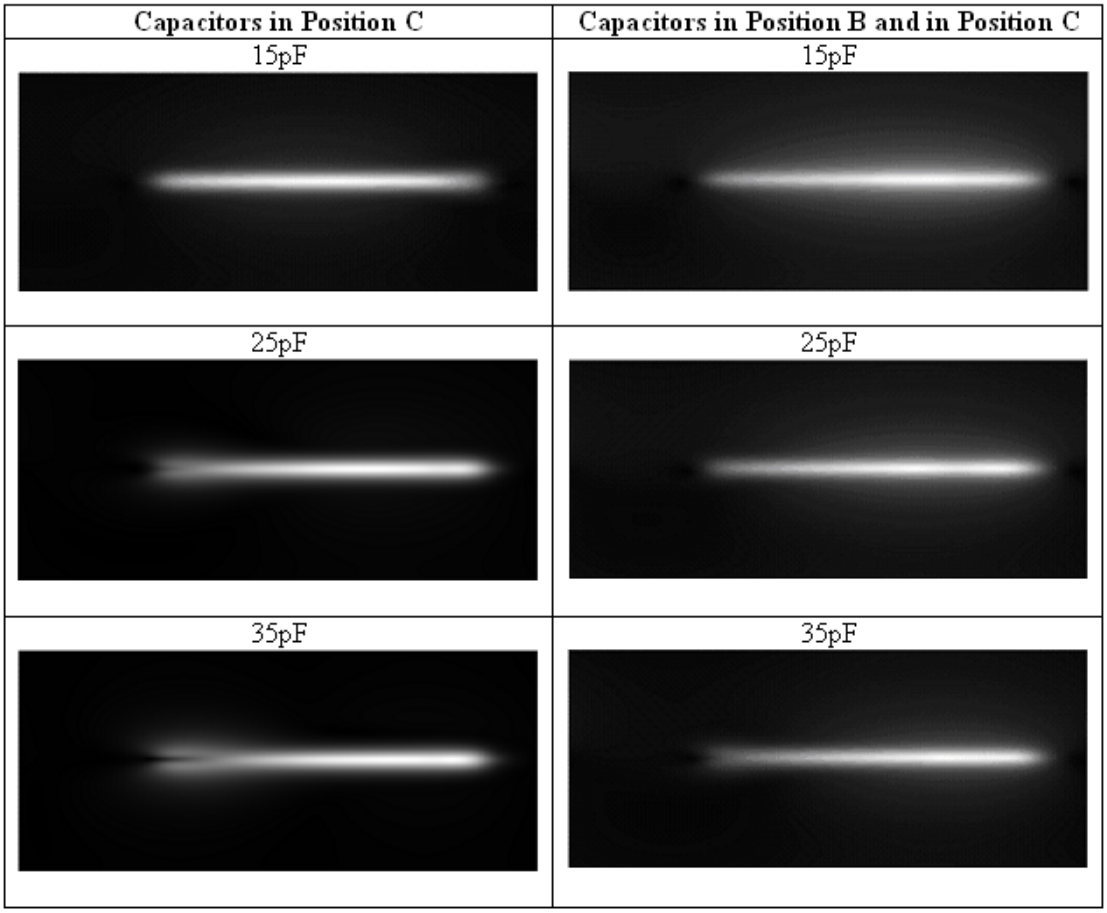

Figure 13: Modeled field magnitude 7mm above the coil with capacitors placed in position C and in both position B and position C.

Table 2 Modeled leg currents on a planar pair coil with 15 pF capacitors inserted on the outside legs at the feed end of the coil.

Leg Currents	Outside Leg 1	Center Leg	Outside Leg 2
Magnitude (feed end)	3.717	7.45	3.717
Phase (feed end)	-88.049	91.964	-88.049
Magnitude (far end)	4.662	9.31	4.662
Phase (far end)	-88.838	91.164	-88.838

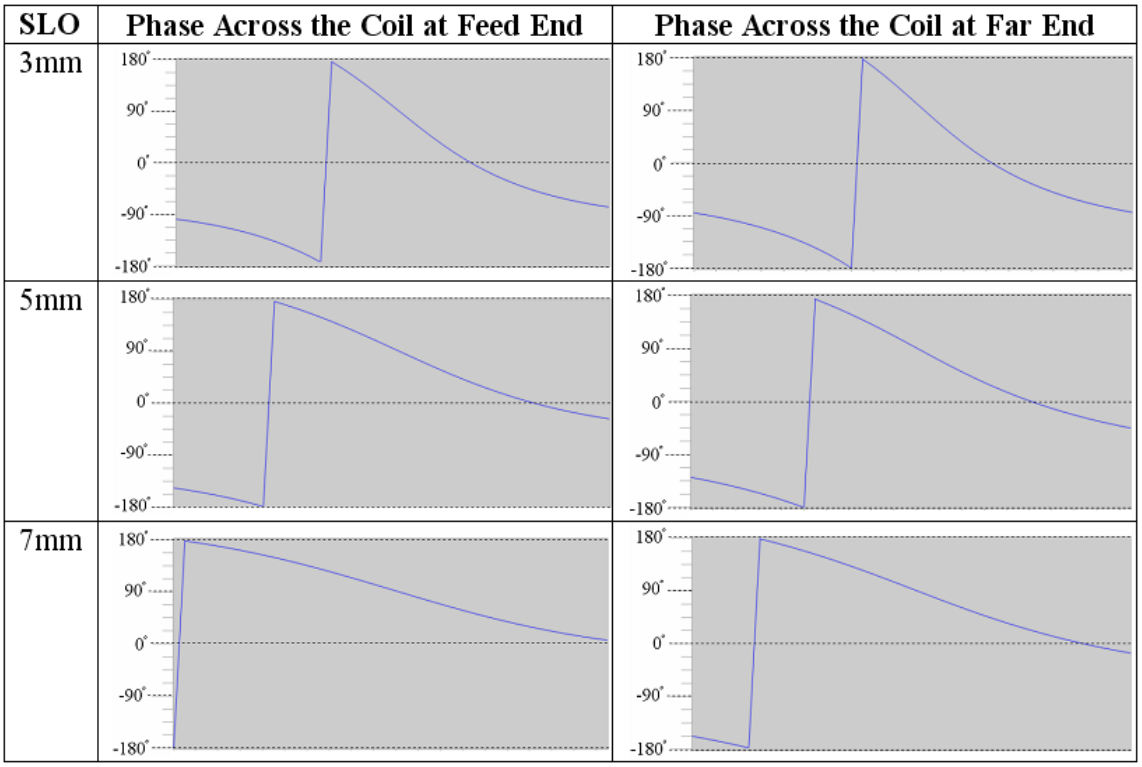

Figure 14: Modeled field phase plots from a planar pair coil with 15pF capacitors placed in position C.

III.2.2 Testing the Proposed Solution

Axial images taken with the normal planar pair and the modified planar pair can be seen in Figure 15; the images from the normal coil demonstrate the artifact, and the images from the modified coil show that the modifications have successfully removed any trace of the artifact. To ensure that the capacitors did not impair the SNR of the planar pair coil profiles through the axial images from both coils were taken at three locations along the coil (Figure 16). The modified planar pair exhibits greater SNR than the normal planar pair coil. The slightly diminished SNR apparent in the images from

the feed end to the far end is a result of the volume coil's lower SNR at the far end of the coil and not the planar pair itself.

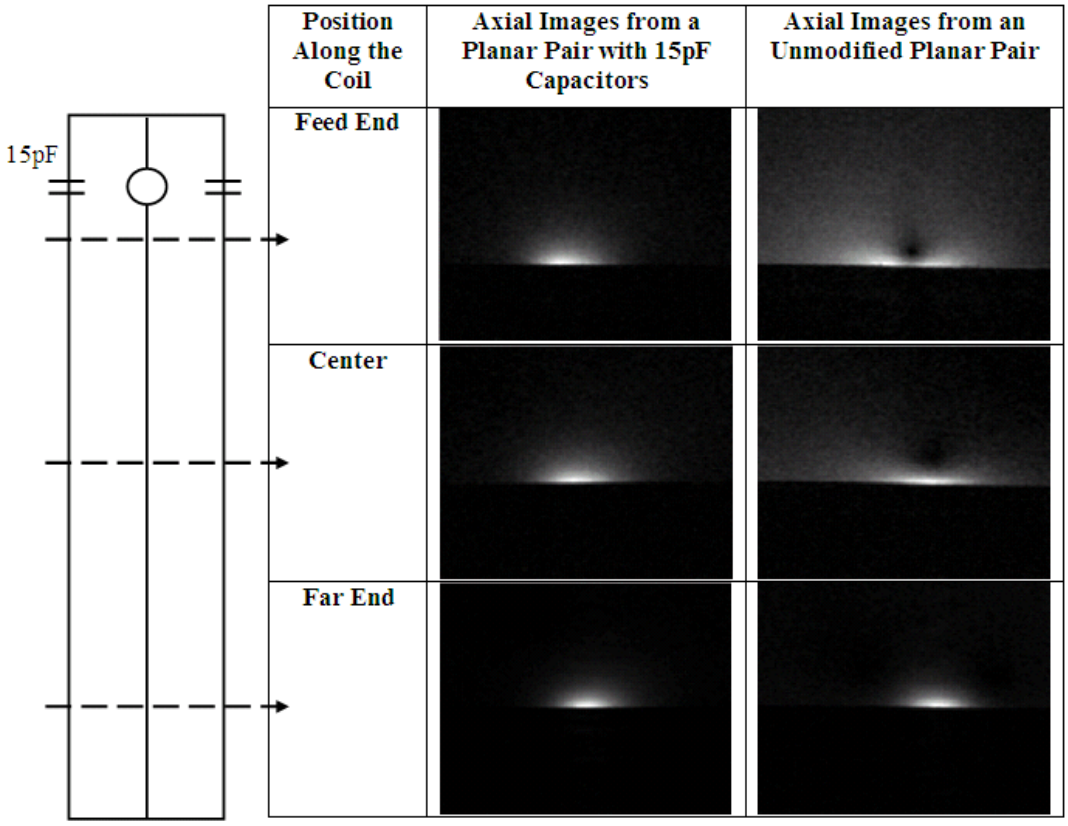

Figure 15: Axial images from an unmodified planar pair and a planar pair with 15pF capacitors inserted at the feed end of the outside legs. The unmodified planar pair images show the artifact at the feed end, while the images from the planar pair with capacitors are artifact free.

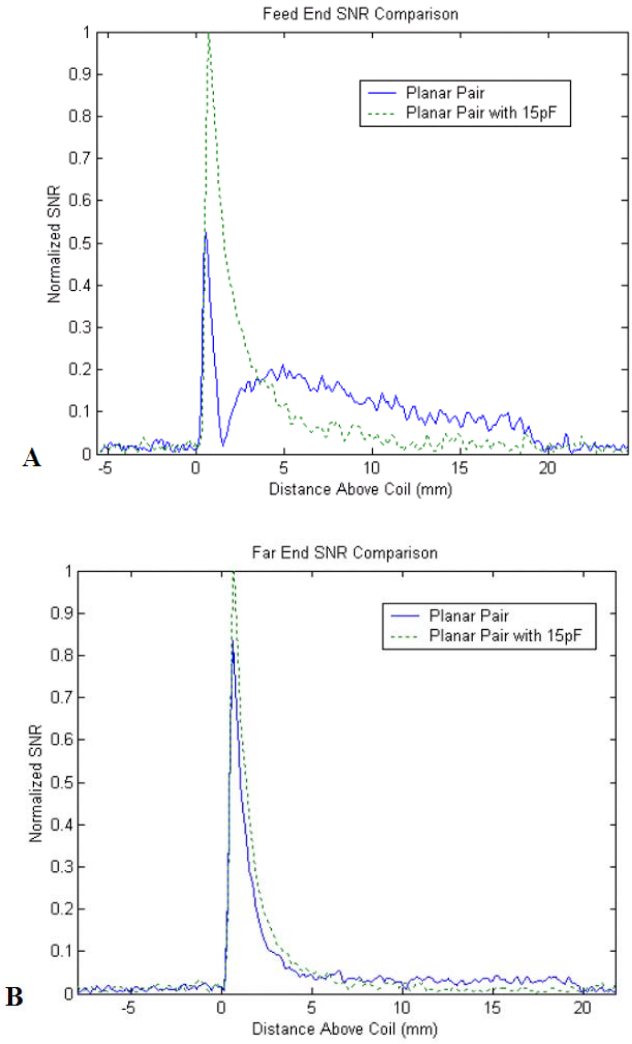

Figure 16: SNR comparison between an unmodified planar pair and a planar pair.

Next, images were acquired from individual channels in the modified 64-channel array; initial images showed unexpected coupling between coils that did not appear in bench measurements. After careful investigation, it was determined that this coupling was due to the excitation of the loop mode in the surrounding coils. This mode did not resonate in the original SEA coil, but the addition of the capacitors to the outer legs

caused it to be resonant and therefore couple to the neighboring coils. In order to prevent the loop mode from being resonant, a short was placed between the two outer legs, directly above the capacitor. This greatly reduced the size of the resonant loop mode but did not interfere with the proper planar pair mode because the outer legs are at the same potential at these points. An artifact-free image from a center element in the array can be seen in Figure 17.

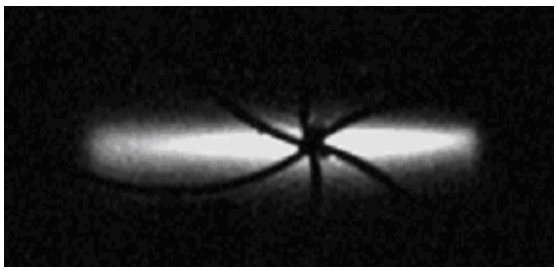

Figure 17: Image from a center element of the 64-channel array. This image demonstrates that no artifact is present and that there is minimal coupling between neighboring coils.

III.3 Conclusions

The reported artifact has been resolved by adding 15pF capacitors to the feed end of the outer legs of the planar pair coil. This solution has also been implemented in the array, with an additional short needed above the capacitors to prevent excitation of the loop mode in neighboring coils. Although the artifact has been successfully resolved, the penetration of the planar pair coil array is still lower than is desired for SEA imaging applications.

CHAPTER IV

LOOP COIL

To expand the applications of SEA imaging it is desired to find an element that has deeper penetration than the planar pair. While the loop coil has deeper penetration than the planar pair coil, it is significantly more complicated to implement. The following chapter describes the investigation of the loop coil for use in SEA imaging. This investigation consists modeling the loop coil, constructing and testing a balun for use with loops at the SEA scale and attempting to decouple loop coils.

IV.1 Procedures

IV.1.1 Modeling the Currents on the Loop Coil

To ensure that the loop coil did not have any unexpected artifacts at 200MHz, similar to the planar pair coil, a 3.3mm wide, 9cm long loop with a trace width of 0.25mm was modeled at 2 MHz and at 200MHz using the in-house full wave modeling program. A dielectric constant of 4.6 was used to simulate the coil substrate, G10; a thin layer of plastic (ε_r=2.2) and water were placed above the coil to simulate the phantom. These currents were then used to model the magnetic field produced by the coil, and the magnitude of the field was plotted thru various planes across the coil. Like the planar pair coil at 200MHz, the modeled currents of the loop at 200MHz showed an increase in current magnitude indicative of a full wave effect. Capacitors were again added to the loop and the fields were recomputed to determine the currents which produced the optimal fields. Finally, imaging was done to verify the modeling results.

IV.1.2 Balanced Feed

Although the loop element is known to have deeper penetration than a comparably sized planar pair, it does come at the expense of being significantly more complicated to implement in a SEA array. Once the currents on the loop coil were optimized, the next complication that was addressed was to produce a balanced feed for the loop coil since the coaxial cable that is used to feed the loop coil has an inherently unbalanced feed. This feed produces stray currents on the ground line making it very difficult to match and tune the loop and creating non-symmetric coil radiation patterns. Typically, a balun is placed at the coil to ensure that the voltage at the loop terminals is 180 degrees out of phase, thus creating a symmetric coil pattern (*33*). Typically, baluns are at a much larger scale than is practical for SEA imaging so it was necessary to develop a miniaturized balun. The balun that seemed the easiest to reduce to the scale necessary for SEA imaging was the lattice balun. The design equations and the circuit diagram for the balun at 200MHz can be seen in Figure 18. The balun is typically constructed with variable air-core inductors and chip capacitors, but these components are too large to be practical for SEA imaging. Instead, a lattice balun was constructed using the 39nH chip inductors (1008HQ series Coilcraft) and 16.1pF capacitors (100B series American Technical Ceramics) and is seen in Figure 19. The width of the lattice balun was 1cm, the maximum size possible to fit 32 baluns in the 16cm available in the magnet for the matching and tuning networks.

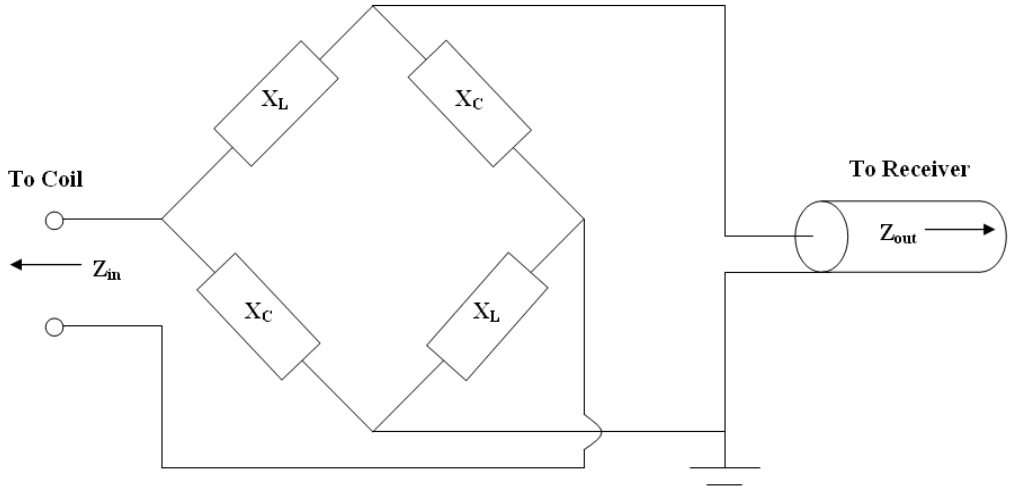

$$X_L = X_C = (Z_{in} * Z_{out})^{1/2}$$

Figure 18: Lattice balun schematic and design equations. The capacitor and inductor values at 200MHz for Zin=Zout=50Ω are 16pF and 39nH.

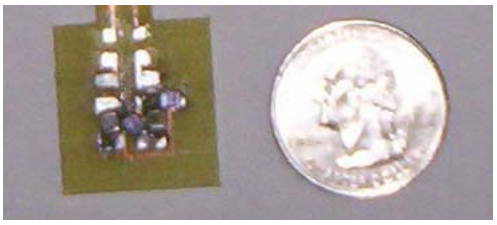

Figure 19: Lattice balun constructed using CoilCraft 1008HQ series 39nH chip inductors and ATC 100B series 16pF capacitors.

IV.1.3 Loop Decoupling

The next issue that was addressed was the severe coupling between loops. As mentioned in II.2, techniques such as overlapping neighboring loops or using transformers between neighboring loops can be used to reduce the mutual inductance.

These techniques have never been reported on coils at the SEA scale, however. Also, as described in II.2, low impedance preamplifiers can be used to further reduce the coupling between coils. The drawback to using preamplifier decoupling, however, is that it only decouples the coils during receive mode. Since it is desired to find an element for SEA that can be used in both transmit and receive, it would be preferred to avoid using preamplifier decoupling.

To determine if any of the above decoupling techniques could be implemented on coils at the SEA scale, two 3.3mm wide loop coils with a separation of 0.5mm and a trace width of 0.25mm were constructed using the C30 PC board prototyper. A coil width of 3.3mm was selected because a future array configuration for SEA is to use two 32-channel arrays in a stacked arrangement; therefore, the elements in this configuration can be twice as wide as the current SEA elements. A larger gap was selected between elements to allow for easier decoupling and to have more space to place transformers between the loops. Cable trap baluns were used on each coil to provide a balanced feed, and the loops were individually matched and tuned using 1-5pF match and tune capacitors. Various overlap configurations and transformer configurations between the loops were experimented with to try to reduce the coupling between coils.

IV.2 Results

IV.2.1 Modeling the Currents on the Loop Coil

The modeling results showed that the currents on the loop at 2MHz were uniform, as expected, but that the currents at 200MHz were much stronger at the far end

of the loop, indicative of a full wave effect. Capacitors were added at various positions along the loop at 200MHz to produce a more uniform current distribution and field pattern. The arrangement which produced the best field pattern was placing a 6pF capacitor at the far end of the loop. The normalized field magnitude taken along the length of the loop at one coil width above the loop at 2MHz, at 200MHz, at 200MHz with a 6pF capacitor inserted taken can be seen in Figure 20. The normalized field magnitude taken across the loop at the feed end and at the far end, one coil width above the loop can also be seen in Figure 20 for the loop at 200 MHz and at 200MHz with a 6pF capacitor. To verify the modeling results, axial images were taken at the feed end of a loop coil with and without a 6pF capacitor. SNR profiles taken from the images can be seen in Figure 21. It is evident from the modeled data and from the images that adding a capacitor to the loop reduces the full wave effects and improves the fields of the loop.

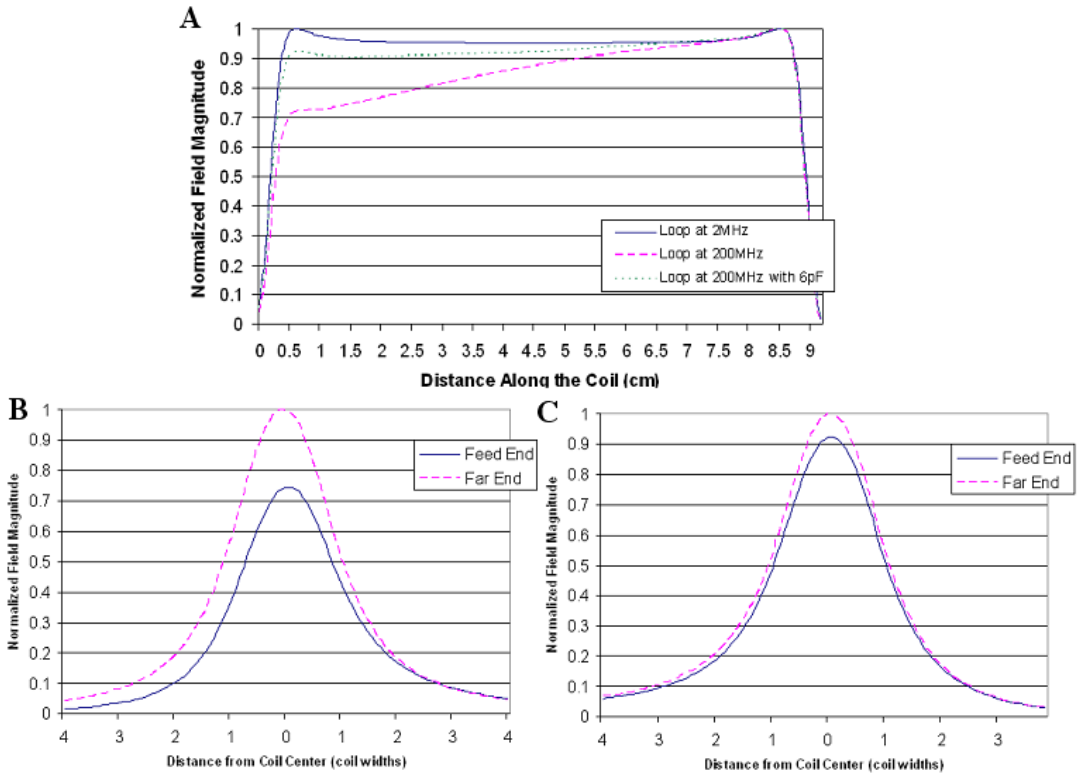

Figure 20: Normalized field magnitude at one coil width above the loop. (A) Along the length of the loop, (B) across the loop at 200MHz and (C) across the loop at 200MHz with a 6pF capacitor placed at the far end of the loop demonstrating that the field is more uniform with the capacitor.

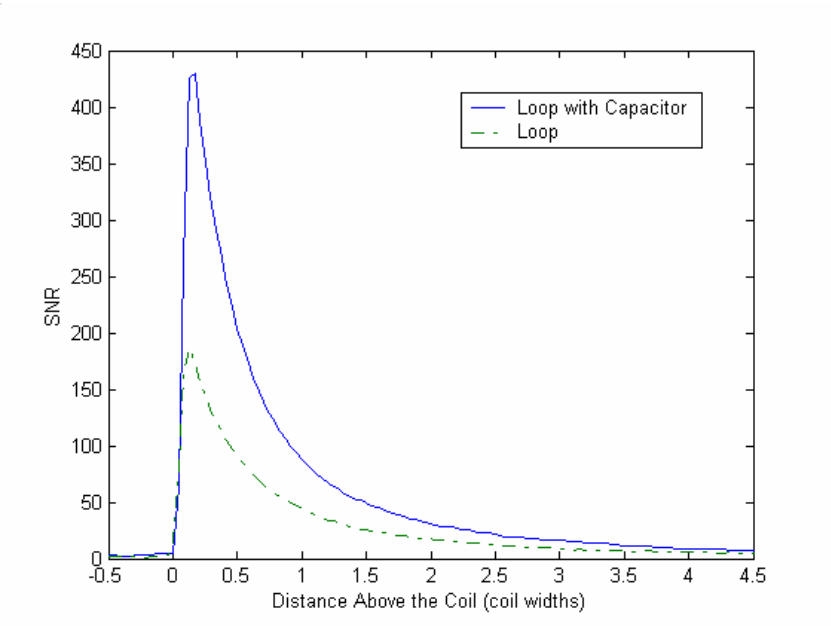

Figure 21: SNR profiles thru axial images from a loop coil with and without a 6pF capacitor.

IV.2.2 Balun

The lattice balun shown in Figure 19 did not sufficiently impede currents on the ground shield of the coaxial cable and does not appear to be a viable option for a miniaturized balun. This failure is attributed to the low Q of the lumped elements and to the lack of variability in the lumped element component values. Future work is needed to investigate the possibilities of miniaturizing other types of baluns.

IV.2.3 Decoupling Results

Both loop coils were individually matched and tuned to 50Ω at 200MHz using the HP 4195A network analyzer. Next, the coils were placed side-by-side and a mode

split of 16MHz was observed. Different amounts of overlap between the coils was achieved by attaching pieces of flexible insulated copper to each loop and changing the shape of the loops to try to decrease the mode split. This was not successful in reducing the mode split below 12MHz, however, and it was difficult to alter the shape of the overlap without tearing the coil traces. Next, various sized transformers were wound and attached between the coils but the mode split was not reduced. Due to the small trace width, 0.25mm, it was very difficult to attach and to manipulate the transformers without damaging the coil. Although much time was spent attempting to reduce the mode splitting between the loops, these attempts were not successful on the loops at this small scale.

IV.3 Conclusions

Miniaturized lattice baluns were tested and constructed but failed to sufficiently impede the coaxial shield currents and to produce a balanced feed. Various decoupling schemes to cancel the mutual inductance between the loops were tested on loops at the SEA scale without success. Due to the long and narrow size of the coils and also the narrow conductor width, these methods were difficult to implement and unsuccessful.

CHAPTER V

STRIPLINE COIL

An 8-channel stripline array, approximately 20 times larger than required for the SEA scale, with at least 19 dB of decoupling between elements has been reported (19). This reported stripline element seems ideal for SEA coil arrays because it does not require a balun and its elements can be decoupled using capacitance, allowing it to be more easily fabricated on the SEA scale. The following chapter describes the investigation of the stripline coil for use in SEA imaging; this investigation consists of constructing stripline elements at the SEA scale, decoupling them from one another and testing their performance in an array.

V.1 Procedures

V.1.1 Two Coil Experiments

To determine the feasibility of the stripline coil for use in SEA imaging stripline coils were built and coupling measurements were made. The first step in building coils was to determine the overall dimensions of a stripline array and therefore the necessary individual element size. To fit within our current volume coil and in our 4.7 T system, the stripline array dimensions need not exceed 13cm in width by 13cm in length, with a possible 16cm in width for the matching network and tuning network. As demonstrated with the current SEA array, to fit 64 channels in this space with a reasonable gap between elements (at least 0.5mm), the maximum element size is 1.8mm. Since the stripline coils involve a more complex design that must include the top loop, as well as a

wider ground loop, they need to be larger than 1.8mm. An alternative to the 64-channel planar array is to use two, 32-channel arrays in a stacked arrangement; this possibility would work well for the stripline design since its intended use is for arrays with deeper penetration. Therefore, with the need to only fit 32 channels across, an element width of 4.1mm was selected. A schematic of the final dimensions can be seen in Figure 22. Although several lengths were experimented with, the final length of the stripline was 9cm.

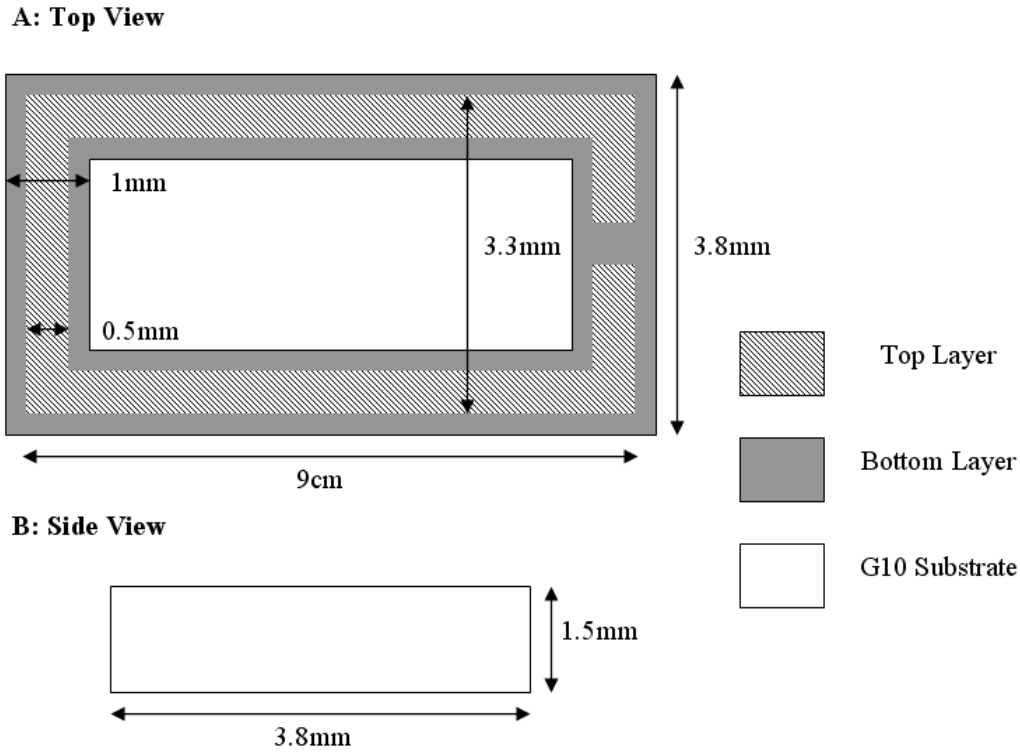

Figure 22: Schematic of a stripline coil showing the dimensions selected to fit 32 channels in a planar array.

Using these dimensions, two side-by-side stripline coils were constructed on 0.75mm and 1.5mm thick glass epoxy (G10) using the C30 PC board prototyper, matched and tuned to 50Ω at 200MHz using the HP 4195A network analyzer and coupling measurements were made. The coils were spaced 0.5mm apart (0.25mm apart between the bottom loops) to provide maximum signal coverage. Capacitors were added between the coils at various positions to try to improve coupling.

V.1.2 Four Coil Experiments

A four element stripline array was constructed on 1.5mm thick G10 to investigate the coupling characteristics in an array environment; the elements in the array were individually matched and tuned and coupling measurements were made. The array was fabricated with the same element dimensions and spacing as the two coil test; the top and bottom of the array can be seen in Figure 23. All four coils have the same match and tune capacitors but varied decoupling capacitors near the feed and far ends of the coil. The via connecting the ground side of the top loop and the bottom loop is also seen. The elements in the array were fed with alternating signal and ground lines, i.e. signal leg, ground leg, signal leg, etc. Alternate four-channel arrays were also constructed to investigate other decoupling schemes. The first was fed with signal and ground pairs, i.e. ground line, signal line, signal line, ground line, etc; the second was constructed with signal and ground pairs but with the second pair flipped 180 degrees, as seen in Figure 24. Coronal images from separate coils from the four-channel array seen in Figure 23 were then acquired to verify that the coil arrays did not exhibit any unexpected coupling and to check for the presence of any field artifacts.

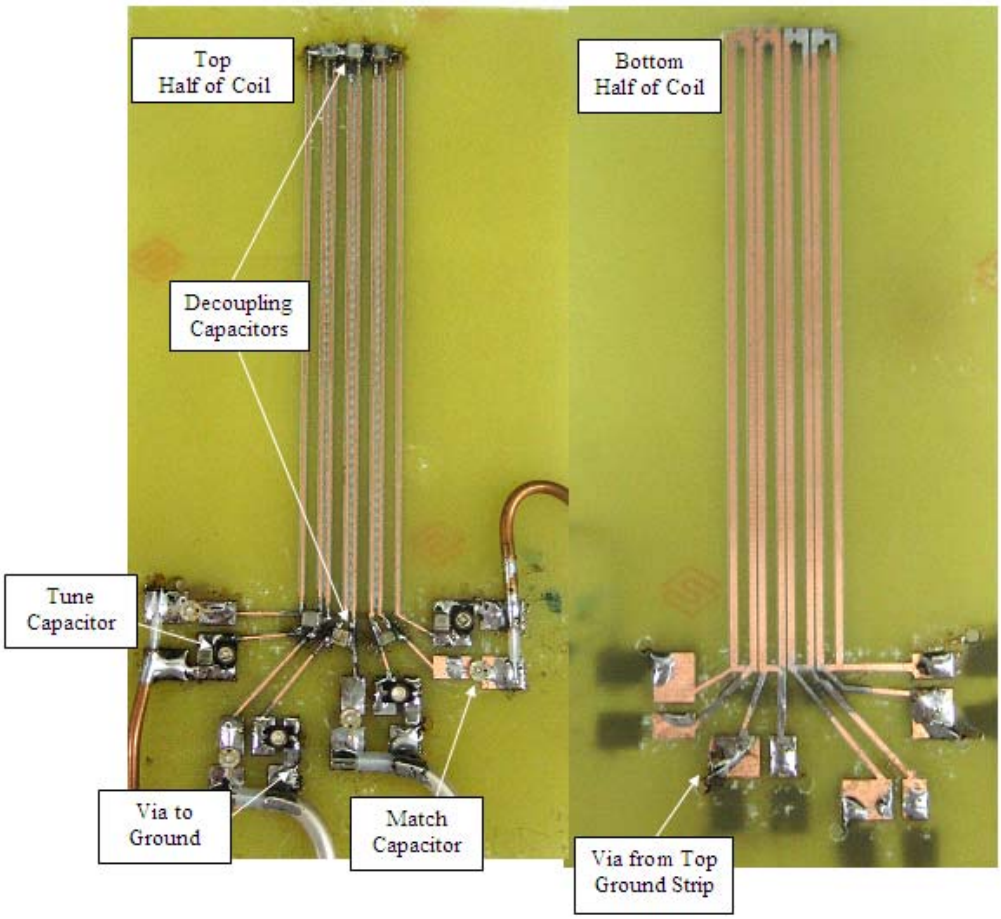

Figure 23: Top and bottom of the 4-channel stripline coil array.

V.2 Results

Initial coupling measurements showed 5 dB of decoupling between unloaded elements fabricated on the 0.75mm thick G10 and only 3.5 dB of decoupling between the coils fabricated on the 1.5mm thick G10. Because the thicker substrate allows for deeper penetration from the same size coil, capacitors were added to it at various positions between the coils to try to improve the coupling. Decoupling of 23 dB was

achieved between the strips with a 5.6pF capacitor placed between the coils at the feed end and a 4.7pF capacitor placed between the coils at the far end. Both coils were matched with 1-5pF variable capacitors and tuned with 5-40pF variable capacitors.

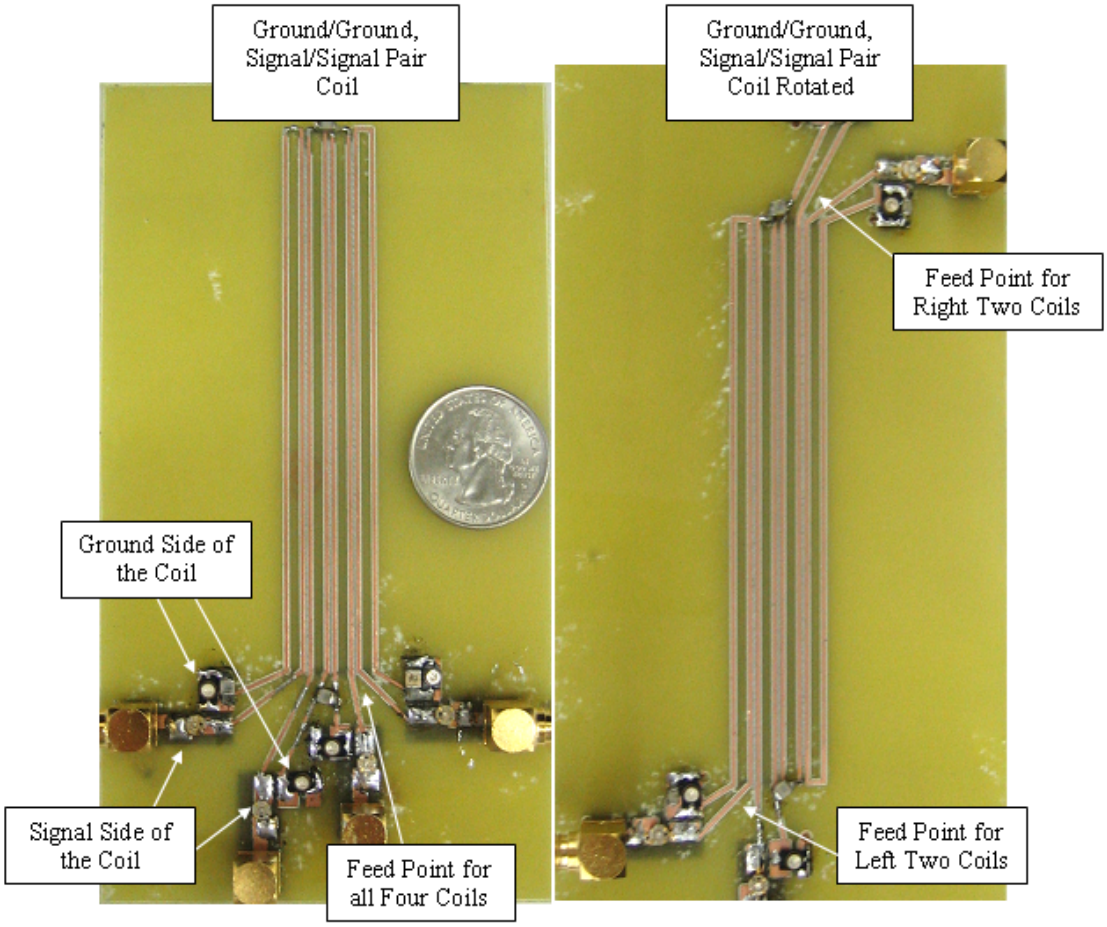

Figure 24: Alternate versions of the stripline coil array.

The four element array with alternating signal and ground lines, seen in Figure 23, exhibited severe coupling between elements without capacitors; once capacitors were added between striplines, the loaded decoupling improved to a minimum of 19 dB

between elements. The capacitance used between elements and the resulting tuning and coupling measurements can be seen in Table 3. All coils were matched with 1-5pF variable capacitors and tuned with 5-40pF variable capacitors. Edge effects increase the required capacitance between coils one/two and three/four as compared to coils two/three; if the array contained more elements, the required capacitance between the center elements should be relatively stable, making fabrication easier. Also, the reported decoupling was achieved by introducing a common ground between the coils at a quarter-wave down from the coil. Shorting the ground lines of the coils at a quarter-wave from the coil creates a high impedance on the ground line, preventing any stray currents on the outside of the ground shield that could increase coupling.

Table 3 Tuning and coupling measurements between coils in the 4-channel stripline array with capacitance placed between neighboring coils. The upper-right corner denotes the tune of each coil and the coupling between coils; the lower-left corner denotes the amount of capacitance placed between coils.

	Coil 1	**Coil 2**	**Coil 3**	**Coil 4**
Coil 1	-21 dB	-24 dB	-28 dB	-26 dB
Coil 2	Feed End: 6.2pF Far End: 6.2pF	-28 dB	-19 dB	-24 dB
Coil 3	None	Feed End: 1.8pF Far End: 2.2pF	-24 dB	-29 dB
Coil 4	None	None	Feed End: 4.7pF Far End: 6.2pF	-26 dB

The four element array with ground/signal pairs, seen in Figure 24, also exhibited favorable decoupling measurements with capacitors. Unlike the first array, however, capacitance only lessened the coupling between adjacent ground lines, i.e. only between the second and third coils. With 2.2pF capacitors placed at the feed end and far end of the coil, the minimum loaded decoupling measurement between coils was 18 dB; the tuning and coupling measurements of the array can be seen in Table 4. The four element array with flipped ground/signal pairs, also seen in Figure 24, exhibited similar decoupling measurements to the non-flipped version, with a minimum, loaded decoupling measurement of 16 dB.

Table 4 Tuning and coupling measurements between coils in the 4-channel stripline array with signal/ground pairs. The upper-right corner denotes the tune of each coil and the coupling between coils; the lower-left corner denotes the amount of capacitance placed between coils.

	Coil 1	**Coil 2**	**Coil 3**	**Coil 4**
Coil 1	-20 dB	-18 dB	-18 dB	-23 dB
Coil 2	None	-23 dB	-20 dB	-18 dB
Coil 3	None	Feed End: 2.2pF Far End: 2.2pF	-38 dB	-25dB
Coil 4	None	None	None	-28 dB

Coronal images from the individual coils in the array showed that the coils in the array environment did not exhibit any unexpected artifacts or unexpected coupling. A

coronal image from the second coil in the array can be seen in Figure 25. The coronal is centered approximately 3mm from the bottom of the phantom.

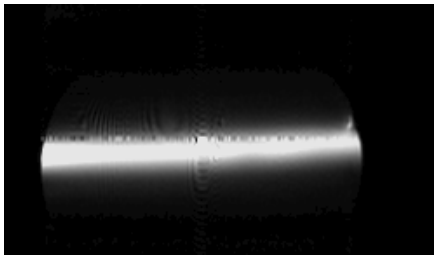

Figure 25: Coronal image from a center element in the four element stripline array demonstrating that there is no significant coupling to neighboring coils.
(TR = 250msec, TE= 28msec, FOV= 12cm, st= 2mm, NA= 1)

V.3 Conclusions

Although the ground/signal pair array seen in Figure 24 exhibited favorable decoupling results, it would be complicated to implement and could require using a more complex phase compensation gradient for SEA imaging. The flipped ground/signal configuration, which exhibited similar performance to the non-flipped version, would be even more difficult to implement and therefore was not pursued any further. The coil configuration seen in Figure 23 exhibits satisfactory decoupling between elements and, due to its simplicity, is the preferred stripline configuration of those configurations tried. The ease of decoupling this array makes it a viable option for SEA imaging.

CHAPTER VI

COMPARISON

The planar pair coil, the loop coil and the stripline coil have been investigated for use in SEA coil arrays. This chapter compares the imaging performance, the coupling, and the complexity of each coil type; the goal of this comparison is to select an element for use SEA imaging with enhanced penetration.

VI.1 Imaging

A single 3.3mm wide, 9cm long planar pair coil, loop coil, and stripline coil was constructed on 1.5mm thick glass epoxy (G10) using the C30 PC board prototyper (Figure 26). The trace width of the loop coil was 0.5mm and the trace width of the planar pair coil was 0.25mm to allow for sufficient spacing between conductors; the dimensions of the stripline coil can be seen in Figure 22. 15pF capacitors were added to each leg of the planar pair coil to prevent any artifacts, as discussed in Chapter III. A 6pF capacitor was added to the far end of the loop coil as discussed in Chapter IV. Back-to-back diodes were added in parallel with the tune capacitor of each coil to prevent the coils from coupling to the transmit coil. Each coil was individually matched and tuned to 50Ω at 200MHz with the HP 4195A network analyzer. Axial images were individually taken with each coil to characterize the coil's performance; a transmit-only birdcage was used for excitation and each coil was used to receive. Magnified axial images from the far end of each coil and SNR profiles demonstrating the penetration depth of each coil can be seen in Figure 27. All of the axial images had the following image parameters: FOV=35mm, repetition time (TR)=500msec, echo time (TE)=28msec, slice thickness

(ST)=3mm, number of averages (NA)=4, resolution in the frequency and phase encode direction (RES)=256, sweep width (SW)=50KHz. To ensure that the SNR seen in the images was representative of the coils actual performance, each image with each coil type was repeated 5 times; the signal and noise from the 5 images was then averaged to produce the SNR profile seen in Figure 27. The images were also repeated on a second day with a similar result. The images and profiles seen in Figure 27 are magnified to half of the original images (FOV=17.5mm). Normalized SNR profiles were also taken from each image at 1mm from the coil's surface to compare the field pattern of each coil (Figure 28).

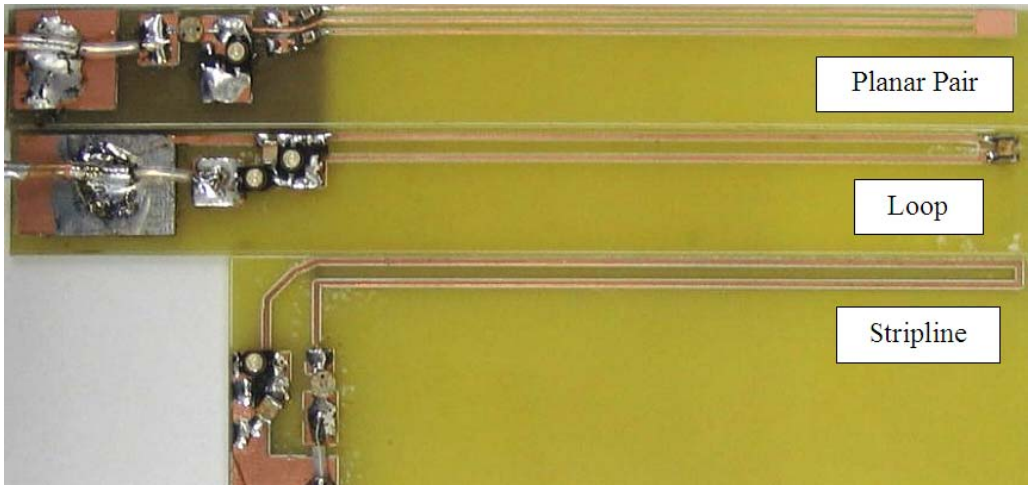

Figure 26: Single 3.3mm wide, 9cm long planar pair, loop, and stripline coils.

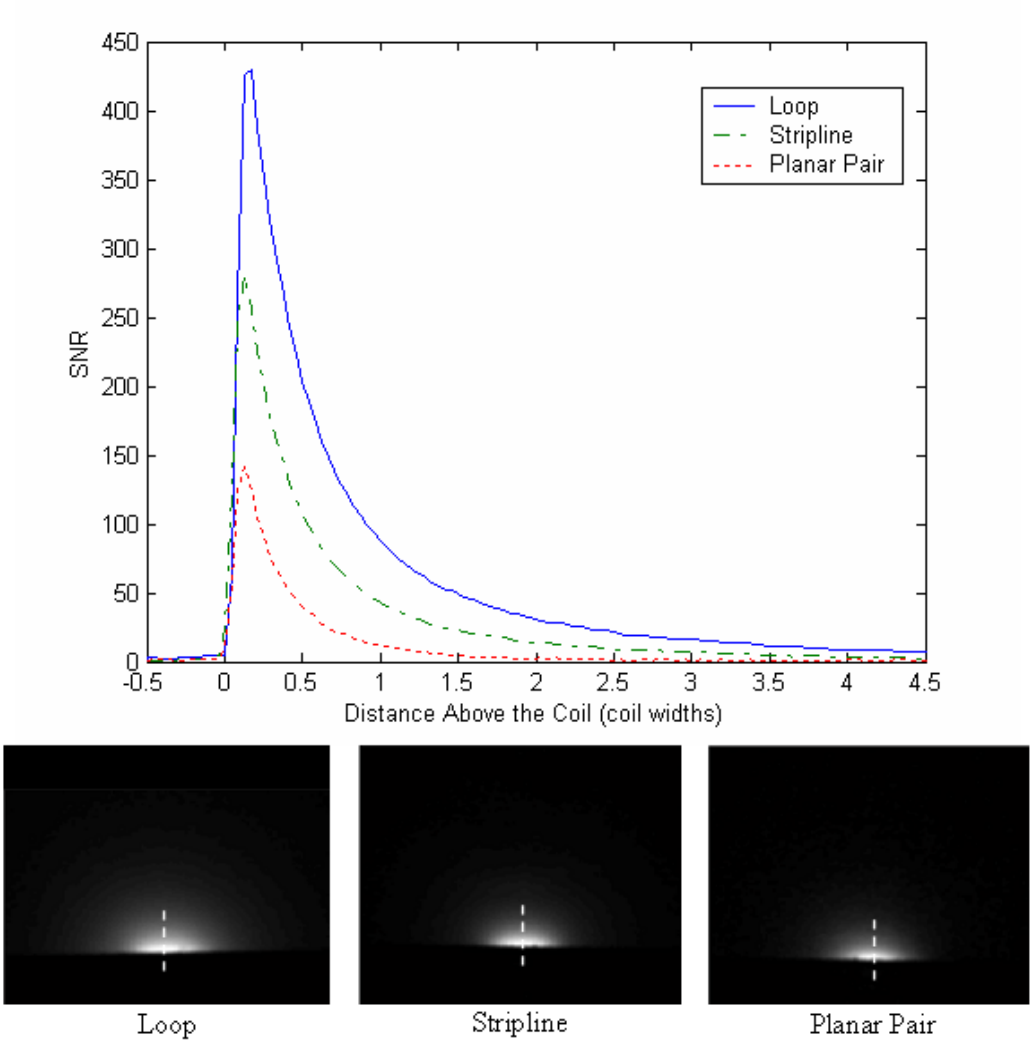

Figure 27: Axial images and SNR profiles from a loop, balun-fed stripline, and a planar pair. The dashed line indicates the approximate vertical line taken through the image for comparison.

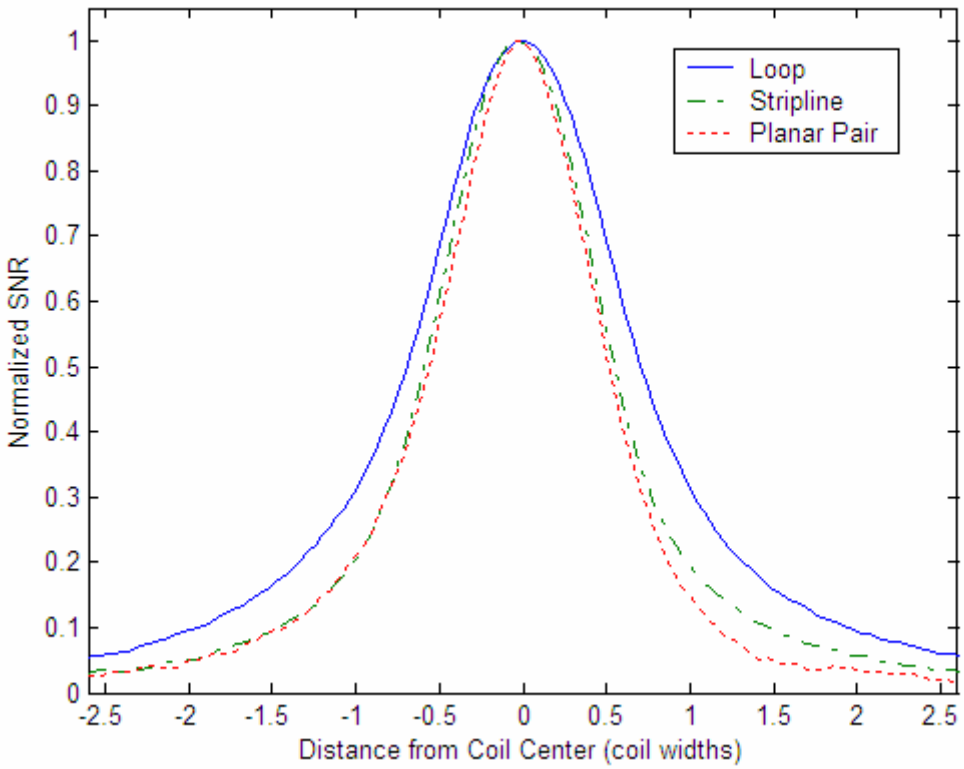

Figure 28: Horizontal profiles taken 1mm above the coil in axial images from the loop, stripline and planar pair demonstrating the narrow field pattern of the planar pair and the stripline coil.

The SNR profiles in Figure 27 demonstrate that the loop coil has the highest SNR near the surface and the deepest penetration. It is worth noting that while the balun-fed stripline coil has less penetration than the loop coil, it has more than twice as much penetration as the planar pair coil at one coil width off of the coil. It is apparent from the normalized SNR profiles in Figure 28 that the balun-fed stripline coil and the planar pair coil have narrower field patterns than the loop coil; not only is this narrowness advantageous for SEA imaging, it also makes the coils easier to decouple.

VI.2 Practical Considerations

SEA requires very long and narrow coils because the resolution in SEA images is determined by the width of the coil element. These long and narrow coils mean that the amount of space available for each coil is very small (<5mm), therefore the coils can not be very complex to implement, including elaborate decoupling schemes between coils or elaborate feed structures.

VI.2.1 Decoupling

Because having coils that receive independent information is vital for any parallel imaging technique, including SEA, it is essential to have the coils in the array decoupled. The planar pair coil can be decoupled from neighboring coils using mutual capacitance between elements (*34*); a similar size planar pair to the one built in VI.1 has decoupled using printed capacitor pads (*26*). The loop coil, however, requires mutual inductance to decouple nearest neighboring coils and low-impedance preamplifiers to control coupling between second and third neighbors. In addition to being much more cumbersome to implement than capacitive decoupling, these decoupling schemes also require the coil to be operated in a receive-only mode since preamplifier decoupling is only possible during receive. This is a major disadvantage to using loop coils, since as mentioned in II.4, it is desired to perform SEA imaging with coils operating in transmit and receive mode due to the phase compensation gradient. As demonstrated in V.2, the stripline coil can be sufficiently decoupled using capacitors. These capacitors could be placed below the array, similar to the artifact solution presented in III.1.2, to decouple the coils without obstructing the imaging region. Because the decoupling scheme relies

only on capacitors, as does the planar pair coil, these coils could be operated in transmit mode and in receive mode.

VI.2.2 Complexity

The planar pair coil does not require a balanced feed and can be fed directly with a coaxial cable. Also, the planar pair coil can be decoupled from its neighbors using mutual capacitance alone. The loop coil does require a balanced feed and therefore needs a balun before it can be fed with a coaxial cable; the loop requires both mutual inductance and low-impedance preamplifiers to decouple it from its neighbors, limiting it to use as a receive only coil. The stripline coil does appear to require a balanced feed, but this has been accomplished by shorting the ground lines of neighboring coils to provide a high impedance on the cables ground preventing any stray currents. Also, the stripline coil can be decoupled using mutual capacitance alone.

VI.3 Conclusions

The loop coil possesses the deepest penetration of all the elements studied, but this penetration comes at the expense of the broadest field pattern, the highest coupling between elements and the most complex feeding scheme that limits the loop to only operating as a receive coil. The stripline coil has a slightly lower penetration than the loop coil but has a narrower field pattern, as desired for SEA imaging. The stripline coil has a simple decoupling mechanism and feed structure that allow it to operate in transmit and receive. The planar pair coil suffers from shallow penetration but is easily decoupled from its neighbors and has the simplest feed structure. Therefore, the stripline coil seems

like the optimal choice for the SEA element, since it has acceptable penetration, fairly simple decoupling scheme, and also can be operated in transmit and receive. The planar pair coil seems like a good choice for SEA surface arrays where not much penetration is required, since it is the easiest to implement.

CHAPTER VII

CONCLUSIONS AND FUTURE WORK

This thesis describes the investigation of several coil elements to determine the best element for SEA imaging with enhanced penetration. This investigation started with modeling the fields of the current SEA element, the planar pair, to eliminate a full wave effect that was causing an artifact in SEA images. This modeling resulted in a solution of adding capacitors to the feed end of the legs of the planar pair to produce more uniform currents on the coil. Images were taken with a single coil with this improvement to prove that the artifact was no longer present. This solution was also successfully implemented on the current 64-channel SEA array.

The loop coil was also investigated as a possible SEA element. The first step in exploring the loop was to model the fields of the loop coil and remove any full wave effects. Next, a miniature lattice balun was built. The lattice balun that was developed did not work at the small scale required for SEA imaging, however. Coupling measurements between loop coils also revealed severe coupling between the loops and extreme difficultly in decoupling the loops.

The stripline coil was also investigated for use with SEA. Coupling measurements were made between stripline coils on various dielectric thicknesses. It was found that two stripline coils on 1.5mm thick dielectric could be decoupled using mutual capacitance. Four element stripline arrays were also decoupled using capacitance when fed with cables shorted at a quarter-wavelength from the coil.

Images taken with a comparably sized planar pair coil, loop coil, stripline coil demonstrated that the loop coil had slightly better penetration than the stripline coil and that the stripline coil and the planar pair coil had the narrowest field patterns. Based on these observations and the simplicity of the stripline, the stripline was selected as the SEA element for applications requiring deeper penetraton.

Recommendations for future work include building and testing a multi-channel stripline array to verify its expected performance and obtaining a modeling program to model the fields on the stripline coil to determine if the stripline also has full wave effects and to determine the optimal dielectric and dimensions for the least coupling between coils but the best penetration. The stripline could also be explored in a non-loop configuration to test the coupling, penetration and need for a balun. Also, a transmit and receive array should be built to test the stripline's performance in transmit and receive.

REFERENCES

1. NessAiver M. 1997. All you really need to know about MRI physics. 1st ed. Baltimore, MD: Simply Physics.

2. Athey TW. 1998. FDA regulation of the safety of MR devices: past, present, and future. Magn Reson Imaging Clin N Am 6:791-795.

3. Hyde JS, Jesmanowicz A, Froncisz W, Kneeland JB, Grist TM. 1986. Parallel image acquisition from noninteracting local coils. J Magn Reson Imaging 70:512-517.

4. Roemer PB, Edelstein WA, Hayes CE, Souza SP, Mueller OM. 1989. The NMR phased array. Magn Reson Med 16:192-225.

5. Hutchinson M, Raff U. 1988. Fast MRI data acquisiton using multiple detectors. Magn Reson Med 6:87-91.

6. Kwiat D, Einav S. 1991. A decoupled coil detector array for fast image acquisition in magnetic resonance imaging. Med Phys 18:251-265.

7. Kelton JR, Magin RL, Wright SM. 1989. An algorithm for rapid image acquisition using multiple receiver coils. Proc SMRM 8:1172.

8. Ra JB, Rim CY. 1993. Fast imaging using subencoding data sets from multiple detectors. Magn Reson Med 30:142-145.

9. Sodickson DK, Manning WJ. 1997. Simultaneous acquisition of spatial harmonics (SMASH): fast imaging with radiofrequency coil arrays. Magn Reson Med 38:591-603.

10. Wright SM, McDougall MP, Kurpad K, Brown DG. 2004. Parallel imaging: system design and limitations. IEEE Intern Symp on Biomed Imaging, Macro to Nano 2:1200-1203.

11. Pruessmann KP, Weiger M, Scheidegger MB, Boesiger P. 1999. SENSE: sensitivity encoding for fast MRI. Magn Reson Med 42:952-962.

12. Griswold MA, Jakob PM, Nittka M, Goldfarb JW, Haase A. 2000. Partially parallel imaging with localized sensitivity (PILS). Magn Reson Med 44:602-609.

13. Kyriakos WE, Panych LP, Kacher DF, Westin CF, Bao SM, Mulkern RV, Jolesz FA. Sensitivity profiles from an array of coils for encoding and reconstruction in parallel (SPACE RIP). Magn Reson Med 44:301-308.

14. Griswold MA, Jakob PM, Heidemann RM, Nittka M, Jellus V, Wang J, et al. 2002. Generalized autocalibrating partially parallel acquisitions (GRAPPA). Magn Reson Med 47:1202-1210.

15. Wright SM, McDougall MP, Brown DG. 2002. Single echo acquisition of MR images using RF coil arrays. Proc EMBS/BMES 24:1181-1182.

16. Lo YT, Wright SM, Navarro JA, Davidovitz M. 2003. Handbook of RF/microwave components and engineering. 2nd ed. New York: John Wiley & Sons.

17. Lee RF, Westgate CR, Weiss RG, Newman DC, Bottomley PA. 2001. Planar strip array (PSA) for MRI. Magn Reson Med 45:673-683.

18. Zhang X, Ugurbil K, Chen W. 2001. Microstrip RF surface coil design for extremely high-field MRI and spectroscopy. Magn Reson Med 46:443-450.

19. Adriany G, Van de Moortele PF, Wiesinger F, Moeller S, Strupp JP, Andersen P et al. 2005. Transmit and receive transmission line arrays for 7 Tesla parallel imaging. Magn Reson Med 53:434-445.

20. Tropp J. 1989. The theory of the birdcage resonator. J Magn Reson 82:51-62.

21. Wheeler H. 1977. Transmission-line properties of a strip on a dielectric sheet on a plane. IEEE Trans Microwave Theory Tech 25:631-647.

22. Wheeler H. 1965. Transmission-line properties of parallel strips separated by a dielectric sheet. IEEE Trans Microwave Theory Tech 13:172-185.

23. Kuester E, Chang DC. 1980. Closed-form expressions for the current or charge distribution on parallel strips or microstrip. IEEE Trans Microwave Theory Tech 28:254-259.

24. Bahl IJ, Trivedi DK. 1977. A designer's guide to microstrip line. Microwaves 16:174-182.

25. Wright SM, McDougall MP. 2004. Single echo acquisition (SEA) imaging at 125 frames per second. Proc ISMRM 12:533.

26. McDougall M. Single echo acquisition magnetic resonance imaging, Ph. D. Dissertation, Texas A&M University, College Station, December 2004.

27. McDougall MP, Wright SM. 2004. Coil phase compensation for single echo acquisition (SEA) imaging. Proc ISMRM 12:330.

28. Brown DG, McDougall MP, Wright SM. 2002. Receiver design for parallel imaging with large arrays. Proc ISMRM 10:863.

29. Wright SM, McDougall MP, Brown DG. 2003. Single echo acquisition (SEA) MR imaging. Proc ISMRM 11:23.

30. McDougall MP, Wright SM, Brown DG. 2003. A 64 channel planar RF coil array for parallel imaging at 4.7 Tesla. Proc ISMRM 11:472.

31. McDougall MP, Wright SM. 2005. 64-channel array coil for single echo acquisition magnetic resonance imaging. Submitted to Magn Reson Med.

32. McDougall MP, Wright SM. 2004. Overcoming phase effects of voxel-sized coils in planar and cylindrical arrays. Proc EMBS 26:1060-1063.

33. Balanis C. 1997. Antenna theory: analysis and design. 2nd ed. New York: John Wiley & Sons.

34. McDougall MP, Wright SM. 2003. Decoupling of planar-pair RF coil arrays using printed capacitance. Proc ISMRM 11:2374.

VITA

Colleen Elizabeth Dominick received her Bachelor of Science degree in Biomedical Engineering, with a minor in Electrical Engineering, from Texas A&M University in August of 2003. Since graduation, she has worked as a Research Assistant under Dr. Steven Wright. She completed her Master of Science degree in Electrical Engineering in August 2005.

Mailing Address: 214 Zachry Engineering Center
3128 TAMU
College Station, TX 77845-3128